The Astronomical Journal, 166:39 (21pp), 2023 August https://doi.org/10.3847/1538-3881/acdacc

Prebiosignature Molecules Can Be Detected in Temperate Exoplanet Atmospheres with JWST

A. B. Claringbold[1,2,3], P. B. Rimmer[4,5], S. Rugheimer[6,7], and O. Shorttle[1,5]
[1] Institute of Astronomy, University of Cambridge, Madingley Road, Cambridge CB3 0HA, UK; alastair.claringbold@warwick.ac.uk
[2] Centre for Exoplanets and Habitability, University of Warwick, Gibbet Hill Road, Coventry CV4 7AL, UK
[3] Department of Physics, University of Warwick, Gibbet Hill Road, Coventry CV4 7AL, UK
[4] Cavendish Astrophysics, University of Cambridge, JJ Thomson Avenue, Cambridge CB3 0HE, UK
[5] Department of Earth Sciences, University of Cambridge, Downing Street, Cambridge CB2 3EQ, UK
[6] Atmospheric, Oceanic and Planetary Physics Department, University of Oxford, Sherrington Road, Oxford OX1 3PU, UK
[7] Department of Physics and Astronomy, York University, 4700 Keele Street, Toronto, ON M3J 1P3, Canada; alastair.claringbold@warwick.ac.uk
Received 2022 November 21; revised 2023 May 13; accepted 2023 May 31; published 2023 July 3

Abstract

The search for biosignatures on exoplanets connects the fields of biology and biochemistry to astronomical observation, with the hope that we might detect evidence of active biological processes on worlds outside the solar system. Here we focus on a complementary aspect of exoplanet characterization connecting astronomy to prebiotic chemistry: the search for molecules associated with the origin of life, prebiosignatures. Prebiosignature surveys in planetary atmospheres offer the potential to both constrain the ubiquity of life in the galaxy and provide important tests of current prebiotic syntheses outside of the laboratory setting. Here, we quantify the minimum abundance of identified prebiosignature molecules that would be required for detection by transmission spectroscopy using JWST. We consider prebiosignatures on five classes of terrestrial planets: an ocean planet, a volcanic planet, a post-impact planet, a super-Earth, and an early-Earth analog. Using a novel modeling and detection test pipeline, with simulated JWST noise, we find the detection thresholds of hydrogen cyanide (HCN), hydrogen sulfide (H_2S), cyanoacetylene (HC_3N), ammonia (NH_3), methane (CH_4), acetylene (C_2H_2), sulfur dioxide (SO_2), nitric oxide (NO), formaldehyde (CH_2O), and carbon monoxide (CO) in a variety of low-mean-molecular-weight (<5) atmospheres. We test the dependence of these detection thresholds on an M dwarf target star and the number of observed transits, finding that a modest number of transits (1–10) are required to detect prebiosignatures in numerous candidate planets, including TRAPPIST-1e with a high-mean-molecular-weight atmosphere. We find that the Near Infrared Spectrograph G395M/H instrument is best suited for detecting most prebiosignatures.

Unified Astronomy Thesaurus concepts: Astrobiology (74); Exoplanet astronomy (486); Planetary atmospheres (1244); Pre-biotic astrochemistry (2079)

1. Introduction

With the recent launch of JWST (see Gardner et al. 2006; Rigby et al. 2023), we are on the cusp of characterizing habitable exoplanets by probing their atmospheric structure, chemistry, and composition. Measuring the abundances of chemical species in exoplanet atmospheres could grant us an understanding of the geochemical and physical processes active on terrestrial exoplanets. Such species include molecules associated with life (biosignatures) and its origins (prebiosignatures). To explain the origin of life on Earth, a number of chemical syntheses have been explored that give rise to promising precursor molecules, such as the Miller–Urey experiment (Miller 1953) and the cyanosulfidic scenario (Patel et al. 2015), to name just two. Molecules that are prerequisites or products of these prebiotic chemistries, for instance, hydrogen cyanide (HCN), may be present in the atmospheres of exoplanets as trace species. Detection of these prebiosignatures could provide insight into how life might arise both on our planet and in the universe (Rimmer et al. 2021b), mitigating the sole example problem in our current understanding of the origin of life. The desire to find these prebiosignature molecules motivates us to explore the capability of JWST to detect and constrain these signatures, and in particular to find the abundance threshold at which this should be possible. This can in turn inform both observing strategies, and the astronomical testability of prebiotic hypotheses, and hence connect the disparate fields of prebiotic chemistry and astronomy.

1.1. Prebiosignatures

Prebiosignatures are molecules that may be involved in prebiotic chemistry, as either the direct products or the feedstock of the pathways themselves (primary prebiosignatures) or molecules created by abiotic processes which may be involved in the origin of life: impacts, volcanism, stellar activity, or lightning (secondary prebiosignatures). For example, the cyanosulfidic scenario uses hydrogen cyanide with UV radiation and a reducing sulfur species, either hydrogen sulfide (Patel et al. 2015) or sulfur dioxide (Xu et al. 2018), to generate RNA and protein precursors. The UV radiation requirements of this scenario place constraints on the astrophysical context in which it can occur. Ranjan et al. (2017) and Rimmer et al. (2018) have explored these astrophysical limits, demonstrating how inactive, cool stars (M and late K dwarfs) have insufficient UV fluxes to drive this chemistry, although flares could mitigate this issue. The abundances of prebiotic species that arise in terrestrial exoplanet atmospheres could also place

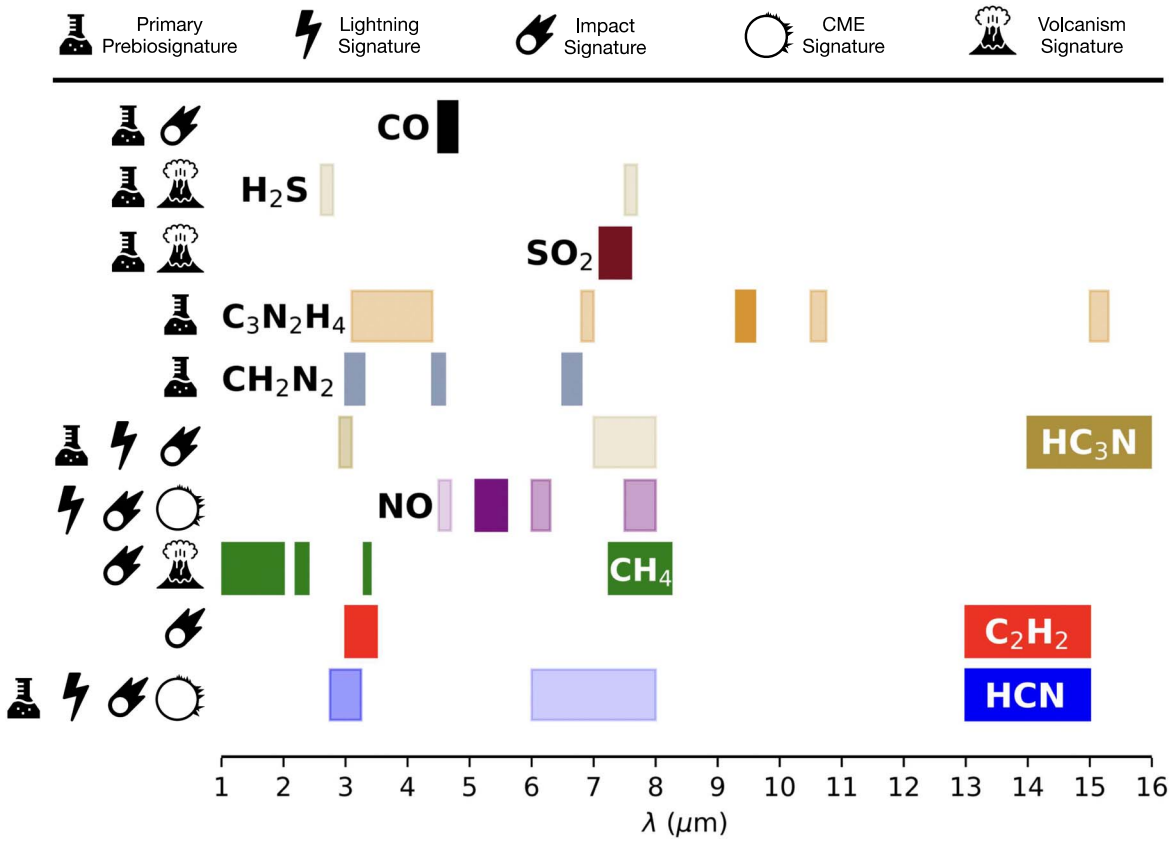

Figure 1. Reproduced from Rimmer et al. (2021b). Primary spectral features of a selection of prebiosignature molecules at JWST-probable wavelengths. The icons represent major physical and geochemical sources of the molecules, with primary prebiosignatures being directly associated with prebiotic chemistry. The species included are carbon monoxide (CO), hydrogen sulfide (H_2S), sulfur dioxide (SO_2), imidazole ($C_3N_2H_4$), cyanamide (CH_2N_2), nitric oxide (NO), methane (CH_4), acetylene (C_2H_2), and hydrogen cyanide (HCN). We include all of these except imidazole and cyanamide in our study. We also investigate ammonia and formaldehyde as potential prebiosignatures. Transparency indicates the strength of the features, with weaker features being more transparent. CME = Coronal Mass Ejection.

constraints on the astrophysical contexts of the origin of life, but are presently less well understood. Hence, there is a need to probe planetary atmospheres for traces of these molecules.

The study of prebiosignatures is a natural extension of the search for biosignatures, and many works have explored the detection of life beyond Earth (e.g., Segura et al. 2005; Kaltenegger et al. 2010; Rauer et al. 2011; Krissansen-Totton et al. 2016; Seager et al. 2016; Rugheimer & Kaltenegger 2018; Alei et al. 2022; Angerhausen et al. 2023; Konrad et al. 2022). The nature of prebiosignatures and our (lack of) understanding of the origin of life draws us to take an open-minded approach, and explore any molecule or process that could support abiogenesis.

Figure 1, from Rimmer et al. (2021b), details major prebiosignature molecules, their sources and their spectral features. We have chosen to focus our analysis on a selection of atmospheric species with wide prebiotic relevance, informed by the cyanosulfidic scenario (Patel et al. 2015) and multiple other prebiotic pathways (e.g., Oró & Kimball 1961; Ferris et al. 1968; Miyakawa et al. 2002; Ferus et al. 2020): hydrogen cyanide (HCN), sulfur dioxide (SO_2), hydrogen sulfide (H_2S), cyanoacetylene (HC_3N), carbon monoxide (CO), methane (CH_4), acetylene (C_2H_2), ammonia (NH_3), nitric oxide (NO), and formaldehyde (CH_2O). The species were also chosen because they are relatively stable molecules that have measured infrared spectra. A brief summary of the relevance of these molecules to prebiotic chemistry follows below.

HCN is central to many prebiotic syntheses (e.g., Oró & Kimball 1961; Sutherland 2016), including homologation to form adenine, one of the purine nucleotides used by life, and the triple bond between the carbon and nitrogen makes it a useful source of accessible chemical energy to form other prebiotically relevant carbon-containing molecules, such as simple sugars, pyrimidine ribonucleotides, and amino acids. HCN was one of the main volatiles produced by Miller's experiment (Miller 1953), and it can be produced by lightning, impacts, and photochemistry (Rimmer & Rugheimer 2019). HC_3N is also the primary feedstock of many pathways (e.g., Ferris et al. 1968; Okamura et al. 2019), providing a chemical "backbone" for nucleotides and a pathway to forming a handful of amino acids. HCN can be produced photochemically, as it occurs on Titan (Clarke & Ferris 1997) and potentially on exoplanet GJ 1132b (Rimmer et al. 2021a). Other scenarios utilize a somewhat reducing atmosphere of CO, along with potentially CH_4 or NH_3, as reagents for prebiotic experiments (e.g., Schlesinger & Miller 1983; Miyakawa et al. 2002). These species can accumulate in an atmosphere due to volcanism from a reducing mantle (Liggins et al. 2022), or from impacts (Zahnle et al. 2020). The sulfur-bearing molecules H_2S and SO_2 have been proposed as important catalysts in the cyanosulfidic (Patel et al. 2015; Xu et al. 2018) and carboxysulfitic (Liu et al. 2021) chemistries, and both are products of volcanism, which itself may be an important component of the origin of life in the form of submarine (e.g.,

Miller & Bada 1988) or surface (Rimmer & Shorttle 2019) hydrothermal vents. Atmospheric C_2H_2 is another feature of impacts (Rimmer et al. 2019), and large impacts can create transiently hydrogen-rich atmospheres (Zahnle et al. 2020; Itcovitz et al. 2022) well suited for prebiotic synthesis (Benner et al. 2020) in terrestrial planets. This is because impacts, and the reduced atmospheres that can result from giant impacts, provide a background chemical environment that can produce large quantities of HCN, possibly HC_3N, and other prebiotically relevant compounds mentioned above. CH_2O is another prebiotically relevant molecule (e.g., Cleaves 2008). It is the feedstock for the formose reaction (Butlerow 1861), a prominent prebiotic scheme that can lead to the formation of several simple sugars used by life (e.g., Schwartz & De Graaf 1993). In addition, formaldehyde reacts with cyanide to produce glycolonitrile, an intermediate that can lead to the production of glycolaldehyde and imidazolide intermediates on the way to RNA and DNA precursors (Patel et al. 2015; Xu et al. 2018; Green et al. 2021) and can also be formed from impacts (Ferus et al. 2019). Nitric oxide (NO) is an important indicator of lightning, stellar activity, and impacts (Mvondo et al. 2001; Airapetian et al. 2016; Heays et al. 2022), and all of these processes can lead to the production of HCN and other prebiotically relevant molecules listed above. It is therefore a potential tracer of physical processes that can lead to the production of life's building blocks.

1.2. Planetary Atmospheres

The atmospheres of exoplanets are observable by transmission spectroscopy (e.g., Charbonneau et al. 2002), secondary eclipse spectroscopy (e.g., Stevenson et al. 2010), and direct imaging (e.g., Konopacky et al. 2013). Critical to our investigation is the ability to retrieve the abundances of particular molecules from the strength of their associated spectral features, for which transmission spectroscopy in the infrared is particularly well suited; hence our focus on JWST for detecting prebiosignatures.

Already with the Hubble Space Telescope (HST) we have detections of atmospheres for super-Earths (e.g., Tsiaras et al. 2016) and even terrestrial planets like GJ 1132b (Southworth et al. 2017; Swain et al. 2021) around M stars. Other HST observations resulted in flat spectra (e.g., Berta et al. 2012), including of GJ 1132b (Mugnai et al. 2021; Libby-Roberts et al. 2022). Such flat spectra are explainable by high clouds (e.g., Kreidberg et al. 2014), high-mean-molecular-weight atmospheres, or a complete lack of an atmosphere. JWST offers a further leap in sensitivity and operates at a favorable wavelength range for molecular absorption features in the near-infrared (NIR) and mid-infrared (MIR) between 1 and 10 μm. This offers an opportunity to explore habitable worlds, particularly around M stars (e.g., Morley et al. 2017; Wunderlich et al. 2021).

Transmission spectroscopy is limited to transiting exoplanets, which represent the majority of known exoplanets, but only a small fraction of all exoplanets. Direct imaging offers the opportunity to explore nontransiting exoplanets, and is better suited to FGK stars (e.g., Des Marais et al. 2002; Rugheimer et al. 2013). Future wide-aperture ground-based telescopes, and potential space missions such as the Near-Infrared/Optical/Ultraviolet telescope proposed by the US Astro2020 Decadal Survey in reflected starlight, and the Large Interferometer For Exoplanets (LIFE) in thermal emission (Quanz et al. 2021), may offer the opportunity to directly explore the atmospheres of Earth-like planets around Sun-like stars and other nontransiting exoplanets. LIFE has sufficient spatial resolution to also be suitable for M dwarfs (Quanz et al. 2022). While both transmission spectroscopy and direct imaging will likely contribute substantially to our observations of exoplanet atmospheres in the future, this work will focus on transmission spectroscopy to play to the strengths of JWST. This means targeting smaller M and K star systems due to the stronger signal of transits around small stars. This comes with both advantages and disadvantages. Habitable zone planets are especially abundant around M stars (Dressing & Charbonneau 2015), but an M-star host also has considerable implications for the habitability and prebiotic chemistry of the planets (Scalo et al. 2007; Shields et al. 2016; Rimmer et al. 2018).

Given how widely anticipated the launch of JWST has been, there have been many studies into its ability to explore exoplanet atmospheres (e.g., Morley et al. 2017; Batalha et al. 2018; Wunderlich et al. 2019). Morley et al. (2017) tested the detectability of Venus-, Titan-, and Earth-like atmospheres of known terrestrial exoplanets at the 5σ level, finding it possible in most cases but expensive in terms of observation times. Notably, seven of the nine planets studied require fewer than 20 transits for the detection of a high-mean-molecular-weight atmosphere. Batalha et al. (2018) calculate that the predominant atmospheric gas is detectable by 10 transits for temperate terrestrial planets around M stars. Of particular relevance to our analysis is the ability to detect trace molecules, and much work has been done on this for biosignatures (e.g., Krissansen-Totton et al. 2018; Schwieterman et al. 2018; Lustig-Yaeger et al. 2019). By far the most promising atmospheres for detection of biosignatures are hydrogen-rich atmospheres (Seager et al. 2013a, 2013b; Schwieterman et al. 2018; Madhusudhan et al. 2021) due to the low mean molecular weight resulting in a puffy atmosphere. Swain et al. (2021) claimed a prebiosignature molecule (HCN) in such an atmosphere around GJ 1132b, although this is disputed (Mugnai et al. 2021; Libby-Roberts et al. 2022). Rimmer et al. (2021a) used this claim along with photochemical models to predict a JWST-detectable abundance of another prebiosignature (HC_3N) in this planet's atmosphere.

Because of the advantages that low-mean-molecular-weight atmospheres present for making molecular detections, we focus on these types of atmospheres on model planets around M stars. We explore the limits that the mean molecular weight, star radius, and observation strategy place on the detectability of prebiosignatures.

1.3. Outline of Work

In this work, we assess the detectability of our selected prebiosignatures in a collection of physically motivated background atmospheres using Bayesian detection tests on simulated JWST transmission spectra. We hope to lay the groundwork for the search for prebiotic environments in the age of JWST by compiling a list of detection thresholds for each prebiosignature molecule. We also present `TriArc`, a versatile and flexible Bayesian detection test tool, for calculating the detection thresholds for atmospheric species in a prescribed background atmosphere.

We describe in Section 2 the creation of a detection threshold pipeline to calculate the minimum abundance of a prebiosignature required for a 3σ detection using radiative transfer

modeling, synthetic JWST noise, and a fully Bayesian detection test targeted on individual spectral bands. Using a multiband approach the abundance of multiple species can be constrained simultaneously. We present the results of our work in Section 3, including model transmission spectra, a library of spectral features of prebiosignatures, and the grid of detection thresholds. In Section 4 we discuss the impacts of planetary and observational properties on the detection thresholds, and briefly consider the consequences of the thresholds for prebiotic chemistry and other planetary processes. In Section 5 we summarize our conclusions and look to the future of observing prebiosignatures.

2. Method

To investigate the detectability of prebiosignatures, we have developed a novel detection test tool `TriArc`, leveraging the forward modeling of the open-source package `petitRADTRANS` (`pRT`; Mollière et al. 2019). We use `pRT` to simulate transmission spectra (Section 2.1), add synthetic JWST noise (Section 2.2), and then perform Bayesian inference against an array of test spectra varying a single parameter, using the statistical framework of `TriArc` to obtain a significance of detection and hence a detection threshold (Section 2.3).

2.1. Atmospheric Models

For the detection tests and atmospheric retrieval, we need to create a forward model of a background atmosphere with a prescribed abundance of a prebiosignature molecule. The transmission spectra of this reference atmosphere is then compared to a set of hypothesis transmission spectra for atmospheres containing various amounts of the prebiosignature. To synthesize these transmission spectra, we calculate the 1D radiative transfer using the correlated-k approximation mode of the `petitRADTRANS`[8] (`pRT`) package (Mollière et al. 2019). For each atmosphere, we use 100 layers of atmosphere equally distributed in log space from 1 μbar down to the surface pressure, and an isothermal temperature profile. We use rebinned opacities at a spectral resolution of $R = 100$. We consider line opacities from the following species: H_2O and CO (Rothman et al. 2010), CO_2 (Yurchenko et al. 2020), CH_4 (Yurchenko et al. 2017), HCN (Barber et al. 2014), NH_3 (Coles et al. 2019), H_2S (Azzam et al. 2016), and C_2H_2 (Chubb et al. 2020); Rayleigh opacities from H_2, He, N_2, CH_4, and H_2O; and collision-induced absorption from H_2–H_2, H_2–He, and N_2–N_2, all included within `pRT`. We also include line opacities from NO (Wong et al. 2017), SO_2 (Underwood et al. 2016), and CH_2O (Al-Refaie et al. 2015) from the ExoMol database (Tennyson et al. 2016), and HC_3N from Rimmer et al. (2021a). We also assume vertically uniform mixing ratios of the atmospheric species.

2.1.1. Background Atmospheres

`TriArc` requires a "background atmosphere" composition, which is held constant during the prebiosignature detection threshold calculation. This includes both continuum opacity sources and line opacities, with abundances dictated by chemical equilibrium or kinetic modeling. It is therefore important for us to present a set of reasonable background atmospheres in which we can test for prebiosignatures. Our own solar system hosts a diverse set of planetary atmospheres, each determined by their planets' distinct geological evolution (e.g., see Pierrehumbert 2010). Venus, Earth, and Titan are all rocky bodies with dense atmospheres, and Morley et al. (2017) used them as models for the detectability of terrestrial atmospheres. However, the atmospheres of Earth and Venus are insufficiently reducing to generate significant RNA precursor prebiosignatures like HCN (Benner et al. 2020). Titan on the other hand is an ideal environment for many prebiosignatures, with species like HCN, C_2H_2, and HC_3N present in the atmosphere (Sagan et al. 1992; Khanna 2005). However, all of these planets have atmospheres poorly suited to detection due to their high mean molecular weights. For an ideal chance of atmospheric characterization, we seek planets with large scale heights (and hence low mean molecular weights, and high temperatures) orbiting small stars (M and late K dwarfs). This can be clearly identified by writing out the effective transit depth, $R_t = R_{\rm pl} + z_{\rm atm}$, where $R_{\rm pl}$ is the radius of planet's surface, and $z_{\rm atm}$ is some characteristic height of the atmosphere at that wavelength (and some function of the scale height, $z_{\rm atm} \ll R_{\rm pl}$). The transmission spectrum is given by the transit depth over the stellar radius R_* squared:

$$\left(\frac{R_t}{R_*}\right)^2 \approx \left(\frac{R_{\rm pl}}{R_*}\right)^2 + \frac{2R_{\rm pl} z_{\rm atm}}{R_*^2}. \quad (1)$$

As the first term is independent of the wavelength, the signal of the transmission spectrum (the wavelength-dependent second term) is seen to be proportional to the atmospheric height $z_{\rm atm}$, which in turn can be related to the atmospheric scale height in hydrostatic equilibrium

$$H = \frac{k_{\rm B} T}{\mu g m_{\rm H}}, \quad (2)$$

where T is the temperature, μ is the mean molecular weight, g is the gravitational acceleration, $k_{\rm B}$ is Boltzmann's constant, and $m_{\rm H}$ is the mass of a hydrogen atom.

Therefore, instead of considering solar system planetary atmospheres, we primarily select planets with atmospheres rich in hydrogen (H_2) and helium (He) so that they have a reduced mean molecular weight. This has already been considered as a promising angle for biosignature analysis (Seager et al. 2013b). We are accustomed to giant planets possessing H_2-dominated atmospheres, but do not see H_2 in the atmospheres of rocky solar systems planets due to the sensitivity of H_2 to hydrodynamic, hydrostatic, and nonthermal escape (e.g., Kasting & Pollack 1983; Lammer et al. 2008; Zahnle & Catling 2017). In order to justify the existence of H_2 in our atmospheric models, we turn to a small number of mechanisms. More massive planets (super-Earths and mini-Neptunes) are capable of retaining primordial H_2-rich envelopes (Fortney et al. 2007; Ginzburg et al. 2016) and could potentially include a liquid water surface (Madhusudhan et al. 2020). Terrestrial planets may be able to retain their primordial atmospheres at greater distances from their star and remain habitable due to the greenhouse effect of H_2 (Pierrehumbert & Gaidos 2011). Volcanic outgassing could also maintain H_2 in the atmosphere (Tian et al. 2005; Ramirez & Kaltenegger 2017; Liggins et al. 2020) and even result in an H_2-dominated atmosphere with a sufficiently reduced mantle (Swain et al. 2021). Zahnle et al. (2020) demonstrated that accretion of reducing iron in the aftermath of an impact can result in a transiently hydrogen-dominated atmosphere.

[8] https://petitradtrans.readthedocs.io/en/latest/

Table 1
Planetary Properties of Model Exoplanets for Prebiosignature Detection Threshold Analysis

Model Planet	Radius (R_{Earth})	Gravity (m s^{-2})	Temperature (K)	Surface Pressure (bar)	MMW	Scale Height (km)
Super-Earth	1.70	13.93	290	1.0	4.60	38
Hycean	2.51	13.56	300	100	2.35	78
Ultra-reduced Volcanic	1.20	10.89	480	1.0	4.51	81
100 kyr Post-impact	1.00	9.81	435	55	2.38	155
10 Myr Post-impact	1.00	9.81	424	45	2.25	160
TRAPPIST-1e/Early Earth	0.91	9.12	246	1.0	29.6	7.6

With the above considerations, we choose the following physically motivated background atmospheres: a Hycean world (ocean planet with hydrogen atmosphere), an ultrareduced volcanic world (active volcanic planet with hydrogen- and nitrogen-rich outgassing), and a post-impact world (planet in the aftermath of a collision with another planetary body resulting in evaporation of the oceans and reduction of atmospheric species by metals from the impacting body) at two different times after the collision. We also include a super-Earth planet similar to that considered by Seager et al. (2013b) to represent a theoretical class of rocky super-Earths with thin hydrogen envelopes that could be formed by outgassing after oxidation of metallic iron by accreted water (Elkins-Tanton & Seager 2008).

The Hycean world is drawn from the planetary properties and atmospheric composition used by Madhusudhan et al. (2021) for the planet K2-18b, constrained by the observations of Benneke et al. (2019). As a potentially habitable planet, K2-18b is a suitable candidate for both prebiosignature and biosignature analysis. The ultrareduced volcanic world is based on the hydrogen-rich outgassed atmosphere modeled by Swain et al. (2021) to explain the detection of HCN in GJ 1132b. The detection is refuted by Mugnai et al. (2021) and Libby-Roberts et al. (2022), but the atmosphere considered is nonetheless prebiotically relevant: photochemical modeling of this ultra-reduced volcanic atmosphere predict an abundance of over 1 ppm of the key prebiosignature HC_3N at 10 mbar (Rimmer et al. 2021a) in addition to HCN. Such an atmosphere is therefore a logical candidate for a more comprehensive analysis. The post-impact planets are based on the modeling of the effects of impacts on the Hadean Earth by Zahnle et al. (2020), considering the atmospheres present at 0.1 Myr and 10 Myr after the impact. Impacts, which lead to substantial amounts of reducing iron (i.e., from the core of the impactor), are proposed as a method for an Earth-like planet to achieve a transient reducing atmosphere and hence a suitable environment for the origin of life (Benner et al. 2020). The post-impact atmospheres we present are end-member cases, being the most reducing possible after the impacts of Zahnle et al. (2020). A variety of processes during the impact can lead to less reducing post-impact environments (Itcovitz et al. 2022). The super-Earth uses an atmospheric composition derived from the photochemical results of Hu et al. (2012).

All the model atmospheres are assumed to be isothermal with vertically uniform mixing ratios, and free from clouds and hazes. The pressure–temperature profile does not have a significant impact on transmission spectroscopy (Morley et al. 2017), but may be overly simplified and introduce bias into the retrieval (Rocchetto et al. 2016). The physical properties of these model planets are displayed in Table 1, and their atmospheric compositions are presented in Table 2. The transmission spectra of these background atmospheres are presented in Figure 2.

We do not want to completely preclude high-mean-molecular-weight atmospheres from our analysis, particularly as the study of the early Earth is important to the understanding of the origin of life, and Earth has possessed a high-mean-molecular-weight secondary atmosphere for most of its history. Furthermore, one of the most promising systems for exoplanetary analysis is TRAPPIST-1 (Gillon et al. 2016), a planetary system with seven terrestrial planets, of which some are in the habitable zone (e.g., Barstow & Irwin 2016; Lustig-Yaeger et al. 2019). Observations suggest that these planets do not possess hydrogen-rich atmospheres (De Wit et al. 2018). Therefore we include an additional model exoplanet, with planetary properties based on TRAPPIST-1e and the atmospheric composition based on a potential early epoch of Earth history (see Kaltenegger et al. 2007; Rugheimer et al. 2015).

For consistency, we model these planets as orbiting a benchmark M4V star with a radius of 0.21 $R_\odot$ (based on GJ 1132) in our initial analysis (Section 3.1). In a subsequent analysis (Section 3.4), we use noise and spectra derived from the Hycean planet orbiting alternative M dwarf targets with different radii and magnitudes: K2-3 and K2-18 (Hardegree-Ullman et al. 2020), LTT 1445 A (Winters et al. 2019), and TRAPPIST-1 (Lienhard et al. 2020), to test the impact of varying these parameters on the detection thresholds. TRAPPIST-1 is modeled with its own spectral type in our analysis of a high-mean-molecular-weight atmosphere for TRAPPIST-1e.

2.2. Synthetic JWST Data

In order to analyze the ability of JWST to detect prebiosignatures, we use the `PandExo`[9] package (Batalha et al. 2017) to simulate realistic noise. For our consistent noise profile to test the impact planetary properties we devise a reasonable observation regime, simulating an M4V star based on GJ 1132 to acquire noise data, as Morley et al. (2017) found GJ 1132b to be a good candidate for transmission spectroscopy. `PandExo` uses the PHOENIX model library (Husser et al. 2013) to simulate observations from stellar inputs.

We simulate at a spectral resolution of $R = 100$, using six total hours of observation per instrument, including three transits (48 minutes each) and a three hour baseline, at 80% full well saturation. We find that using the following instruments to explore the entire wavelength range for 1–10 μm is most effective: Near Infrared Imager and Slitless Spectrograph (NIRISS) Single-Object Slitless Spectroscopy (SOSS; 0.8–2.9 μm), Near Infrared Spectrograph (NIRSpec) G395M (2.9–5 μm), and Mid-Infrared Instrument (MIRI) Low-

[9] https://natashabatalha.github.io/PandExo/

Table 2
Atmospheric Mixing Ratios of Model Exoplanets for Prebiosignature Detection Threshold Analysis

Model Planet	H_2	He	N_2	CH_4	CO	CO_2	H_2O	HCN	NH_3
Super-Earth	90%	0.0	10%	0.0	0.0	1e-4	1e-5	0.0	0.0
Hycean	90%	9%	0.0	5e-4	0.0	0.0	1%	0.0	1e-4
Ultra-reduced Volcanic	90%	0.1%	8.9%	0.3%	0.3%	0.0	2e-5	0.3%	0.0
100 kyr Post-impact	98%	0.0	0.5%	1.76%	0.0	0.0	1e-7	0.0	0.0
10 Myr Post-impact	99%	0.0	0.41%	0.0	0.575%	0.0	1e-7	0.0	0.0
TRAPPIST-1e/Early Earth	0.0	0.0	90%	2e-6	0.0	10%	1e-6	0.0	0.0

Resolution Spectrometer (LRS; 5–10 μm), giving a good noise of 25–80 ppm (see Figure 3). Although its wide spectral baseline makes it attractive for atmospheric characterization, NIRSpec Prism saturates for GJ 1132 and is near or below the saturation limit for many of the other terrestrial planet systems we may consider (Jakobsen et al. 2022). The NIRISS SOSS/NIRSpec G395M combination contains the best information content for characterizing exoplanets orbiting bright stars (Batalha & Line 2017).We use the medium-resolution grism G395M over the high-resolution grism G395H, as the latter possesses a gap in its spectral range between 3.7 and 3.8 μm, which contains relevant spectral information for prebiosignatures.

The approach we take in implementing JWST noise into `TriArc` follows that of Madhusudhan et al. (2021). Using `PandExo` we calculate the sensitivity of the instrument as a function of the wavelength for the different instruments, and add a corresponding amount of Gaussian noise to our synthetic transmission spectra before feeding them into the detection test. We also use `exo-k` (Leconte 2021) to rebin the opacities used in the atmospheric models into the desired spectral resolution of $R = 100$.

We compute a variety of noise profiles to test the sensitivity of the detection thresholds to observational parameters (Section 3.4). The process is the same as described above, except we vary the number of transits and the baseline observation time, which we state in each case.

2.3. Detection Tests

In order to estimate the significance of detection for any particular atmosphere and noise profile, we perform a Bayesian detection test. We have developed `TriArc` for that purpose, using Bayesian inference to retrieve a single parameter (the abundance of a single species) with all other parameters fixed as delta priors. As only a single parameter is retrieved (as opposed to many parameters simultaneously in a full retrieval), the need for more involved sampling approaches is eliminated, greatly improving the speed of our analysis. This allows a large number of detection tests to be performed, which is important for finding the location of the detectability threshold. A realistic retrieval of an observed transmission spectrum would need to fit for every unknown parameter, including the planetary characteristics and atmospheric composition, a much more computationally demanding task. Therefore, the detection thresholds that we obtain from `TriArc` are an order-of-magnitude estimate of what is possible with JWST observations. To verify our detection thresholds, we benchmark our detection tests against full retrievals performed using the retrieval package of `pRT`.

The hypotheses to test with Bayes' theorem are represented by a set of test spectra with different abundances of the species being retrieved. The distribution of these hypotheses is given by a Jeffreys prior with uniform probability in log space, varying the mass fraction from 10^{-11} to 1. The "evidence" is a noisy model spectrum with a prescribed abundance of the retrieved species. All other atmospheric parameters not being retrieved are fixed as delta priors. In order to retrieve the abundance of the species, i.e., assign a likelihood to each hypothesis, the goodness of fit between the noisy model spectrum and each of the test spectra is computed within the wavelength range of the spectral feature of the species being retrieved. The goodness of fit is measured using a Gaussian radial basis likelihood function over a set of data points in wavelength space λ, where E_λ is the model spectrum data point, $H_{i,\lambda}$ is the ith test spectrum data point, and σ_λ is the model noise:

$$P(E|H_i) = \prod_\lambda (2\pi\sigma_\lambda^2)^{-\frac{1}{2}} \exp\left(-\frac{(H_{i,\lambda} - E_\lambda)^2}{2\sigma_\lambda^2}\right). \quad (3)$$

This probability of the evidence given the hypothesis $P(E|H_i)$ is then converted to a posterior probability distribution function (PDF), $P(H_i|E)$, using Bayes' theorem and the aforementioned Jeffreys prior $P(H_i)$:

$$P(H_i|E) = \frac{P(E|H_i)P(H_i)}{\sum_i P(E|H_i)P(H_i)}. \quad (4)$$

The mean and standard deviations of the retrieved abundance can then be calculated from the posterior PDF. The maximum abundance of the species present can be constrained by integrating the PDF: the lowest abundance that when integrated up to gives a value of 99.7% (3σ) is the maximum abundance. To estimate the significance of a detection, the posterior PDF is integrated above a certain fraction of the input (we use 0.01). This is equivalent to working out the probability that you retrieve 1% or more of the abundance you input into the forward model. If this is equal to or greater than 99.7% we label the detection as significant at the 3σ level. The detection threshold is found by adding progressively more of a prebiosignature species until a significant detection is achieved. For an illustrative example of this see Figure 4.

TriArc detection tests can utilize the entire wavelength range of an instrument to calculate the detection threshold of a prebiosignature, combining information from all spectral features. Alternatively, it can narrowly target individual spectral features, which are listed in Table 3.

Using the entire wavelength range of the instrument gives the most optimistic detection thresholds, quoted in Table 4, and more closely matches the methodology of a full retrieval. Targeting individual features results in more conservative detection thresholds, and illustrates the relative strength of features in different backgrounds, and can be used to demonstrate how molecules that share their strongest feature

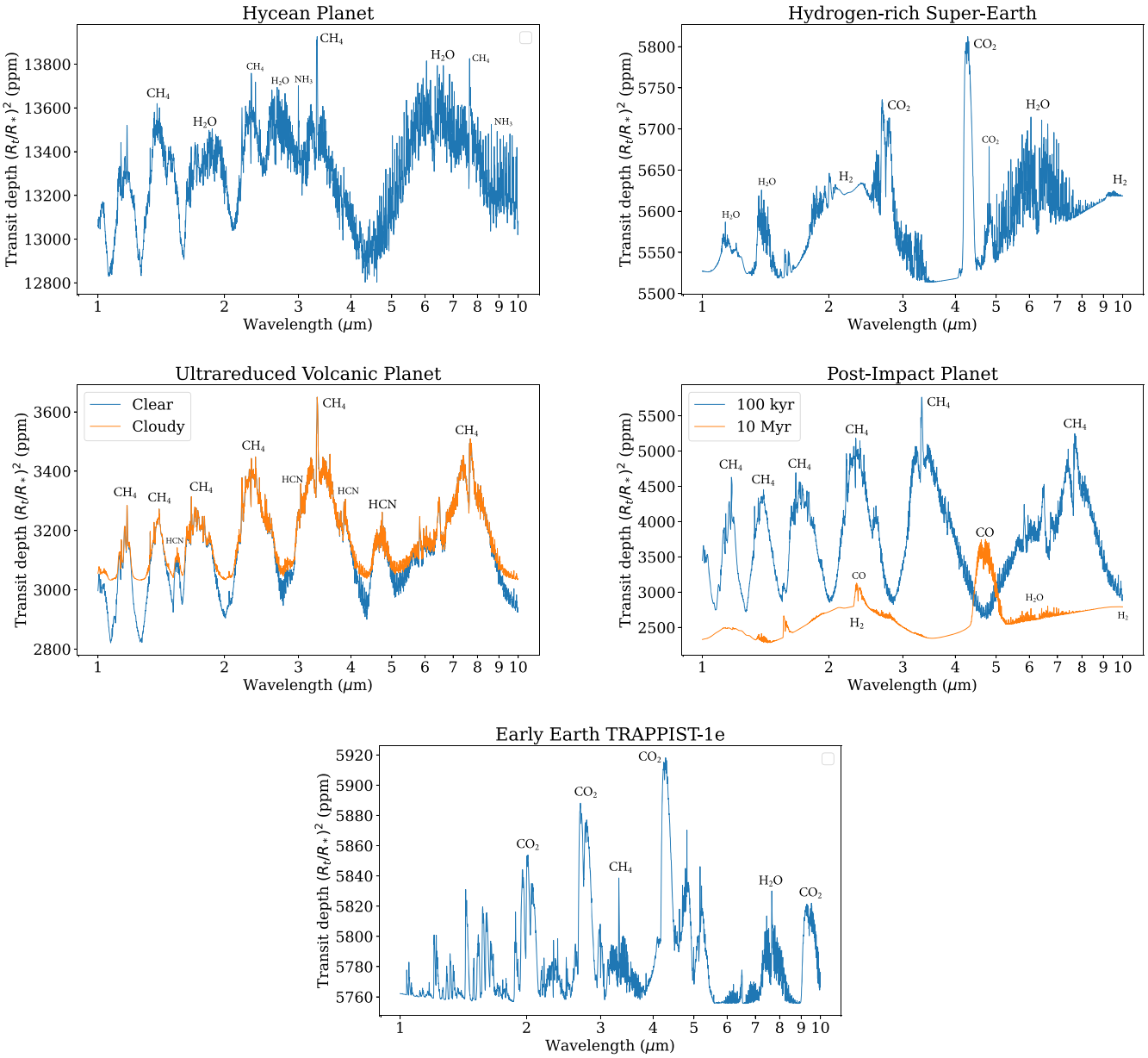

Figure 2. Transmission spectra of model exoplanets, calculated using `petitRADTRANS`. Top left: Hycean planet, with planetary and atmospheric properties chosen to match those described by Madhusudhan et al. (2021) for K2-18b. Top right: Super-Earth with thin hydrogen envelope, with planetary properties chosen to match those of HD 88512b, and atmospheric properties based on the modeling of Hu et al. (2012). Middle left: Ultra-reduced volcanic planet, both with (blue) and without (orange) a gray cloud layer at 10 mbar, with planetary and atmospheric properties chosen to match those described by Swain et al. (2021) for GJ 1132b. Middle right: Post-impact planet transmission spectra 100 kyr (blue) and 10 Myr (orange) after the impact, with atmospheric properties chosen to match those described by Zahnle et al. (2020) for a Hadean Earth. Bottom: Model TRAPPIST-1e with an atmosphere to emulate an early epoch of Earth history (Kaltenegger et al. 2007).

can be distinguished. We do this by defining a disambiguation threshold, the minimum abundance required to distinguish between molecules with overlapping features, which is equal to the detection threshold of a molecule targeted at the strongest nonoverlapping band. The results of this method are presented in Figure 5 and subsequent figures.

3. Results

Here we present a selection of prebiosignature detection thresholds summarized in Figure 5. For each model exoplanet we calculate the detection threshold using a consistent synthetic noise profile based on observing three transits of GJ 1132b (see Section 2.2) to demonstrate the dependence of detection thresholds on planetary parameters. These results are listed in Section 3.1. We include additional results with added gray cloud decks at various altitudes to quantify the impact of clouds in Section 3.2. We benchmark these detection thresholds results against full retrieval results with `petitRADTRANS` in Section 3.3. We also explore the impact of noise profiles from alternative observational regimes on the detection thresholds in Section 3.4. To quantify the observational regime necessary for prebiosignature analysis, we calculate the detection thresholds as a function of the number of observed transits using a model Hycean planet as a benchmark. We extend this by testing the impact of observing different stars for a varying number of transits on the HCN detection threshold in the Hycean benchmark planet. We also do this for our model TRAPPIST-1e with a high-mean-molecular-weight (90% N_2, 10%

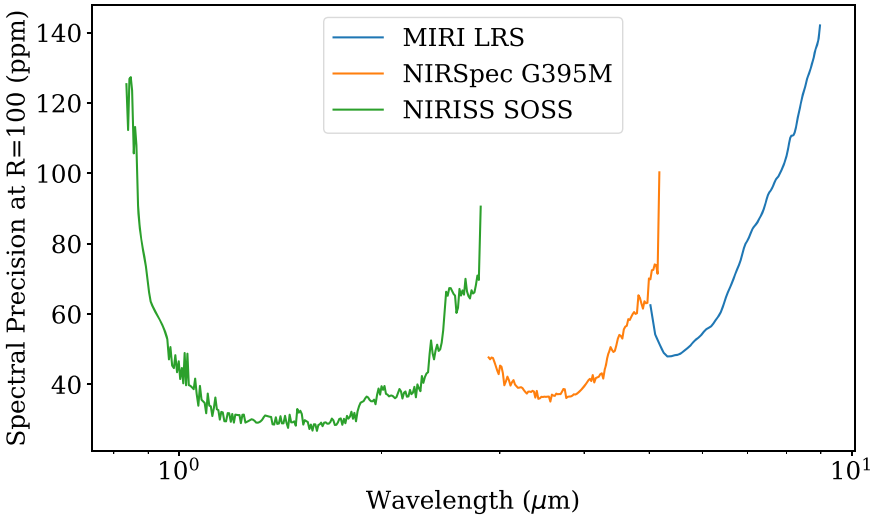

Figure 3. Spectral precision of JWST instruments as a function of the wavelength, at resolution $R = 100$ when observing GJ 1132b for 6 hr per instrument, including three transits, at 80% full well saturation, simulated using `PandExo`.

CO_2) atmosphere. In Section 3.5 we discuss the handling of degeneracies between different prebiosignatures; we introduce disambiguation thresholds, the minimum abundances to distinguish between molecules. The detection thresholds are compiled in Table 4 and illustrated in Figure 5. We explore the sensitivity of our results to temperature, mean molecular weights, planet radius, surface pressure, gray cloud layers, star radius, and instrument precision in the Appendix.

3.1. Detection Thresholds

For our primary observational regime, we calculate the detection thresholds by simulating the transmission spectrum of three transits around GJ 1132 at a spectral resolution of $R = 100$, as described in Section 2.2, for each of the following instruments: NIRISS SOSS, NIRSpec G395M, and MIRI LRS (for a total of six hours of observation per instrument). We find this to be a good compromise between observation time and detection thresholds. This is done for all of the model hydrogen-rich exoplanets. A summary of these results is found in Table 4 and Figure 5. No prebiosignature molecules in the modeled early-Earth exoplanet are detectable with this regime.

Using the primary observation regime, all of the prebiosignatures are detectable in the model Hycean world, with its CH_4- and H_2O-dominated transmission spectrum. Abundances of 0.06 ppm HC_3N, 0.6 ppm SO_2, 4 ppm C_2H_2, 1.3 ppm CO, and 30 ppm HCN are detectable using the NIRSpec G395M instrument. 70 ppm H_2S is detectable by the NIRISS SOSS instrument, and a mixing ratio of at least 400 ppm NO is detectable using MIRI LRS. CH_4 and NH_3 are present in chemical equilibrium in this atmosphere and are hence considered as background species. The spectral feature of CH_2O at 6 μm, required to distinguish it from CH_4, is detectable at 16 ppm with MIRI LRS. We also use the Hycean planet as a benchmark for alternative observational regimes (Section 3.4).

The hydrogen-rich super-Earth, with its CO_2 and H_2–H_2 transmission spectrum, is very well suited to most prebiosignatures molecules, despite it having the lowest scale height of the planets we consider, due to the lack of absorbing molecules in the important region around 3 μm. Abundances of 0.02 ppm of CH_2O, 0.14 ppm of HC_3N, 0.5 ppm of CH_4, 0.6 ppm C_2H_2, 7 ppm NH_3, 2 ppm of HCN, 0.5 ppm SO_2, 2 ppm of CO, and 30 ppm of H_2S are all detectable with NIRSpec G395M. NO is detectable at 60 ppm with MIRI LRS. Our resultants are concordant with Huang et al. (2022), which finds a detection threshold of 5 ppm for ammonia in a hydrogen-dominated super-Earth atmosphere.

The ultrareduced volcanic planet, despite having a similar scale height to the Hycean world, has generally worse detection thresholds due to high concentrations of strongly absorbing CH_4 and HCN in the atmosphere. In a clear atmosphere, abundances of 6 ppm HC_3N, 14 ppm of SO_2, 60 ppm of C_2H_2, and 80 ppm NH_3 are detectable with NIRSpec G395M. CH_4 and HCN are part of the background atmosphere due to the ultra-reduced outgassing. NO is detected with MIRI LRS for an abundance of at least 900 ppm, and the 6 μm feature of CH_2O for an abundance of 8 ppm. A 130 ppm mixing ratio of H_2S is detectable with NIRISS SOSS, and a 100 ppm mixing ratio of CO with NIRSpec G395M.

The post-impact planets, with their high-temperature, hydrogen-dominated atmospheres, have the highest scale height, and are hence the best suited to detection. In the CH_4-dominated spectrum of the 100 kyr post-impact Hadean Earth, we could detect 150 ppb HC_3N, 1.4 ppm C_2H_2, 0.5 ppm CO, 7 ppm NH_3, 4 ppm SO_2, and 4 ppm HCN using NIRSpec G395M, 40 ppm H_2S using NIRISS SOSS, and 1.3 ppm CH_2O and 40 ppm NO using MIRI LRS.

The 10 Myr post-impact transmission spectrum is instead dominated by the lower opacities of CO and H_2–H_2, resulting in low detection thresholds that enable trace abundances of prebiosignatures to be detected: 0.8 ppb CH_2O, 7 ppb HC_3N, 9 ppb CH_4, and C_2H_2, 26 ppb HCN, 30 ppb SO_2, and 1.3 ppm of H_2S all using NIRSpec G395M. Also detectable is 0.4 ppm of NO with MIRI LRS.

3.2. Impact of Clouds

In the case of both the hydrogen-rich super-Earth and the 10 Myr post-impact planet, the overall opacity is very low, with the transmission spectrum reaching deep in the planetary atmospheres to where the continuum H_2–H_2 opacity becomes optically thick. In this case, any source of higher-altitude opacity, including clouds and aerosols, would massively

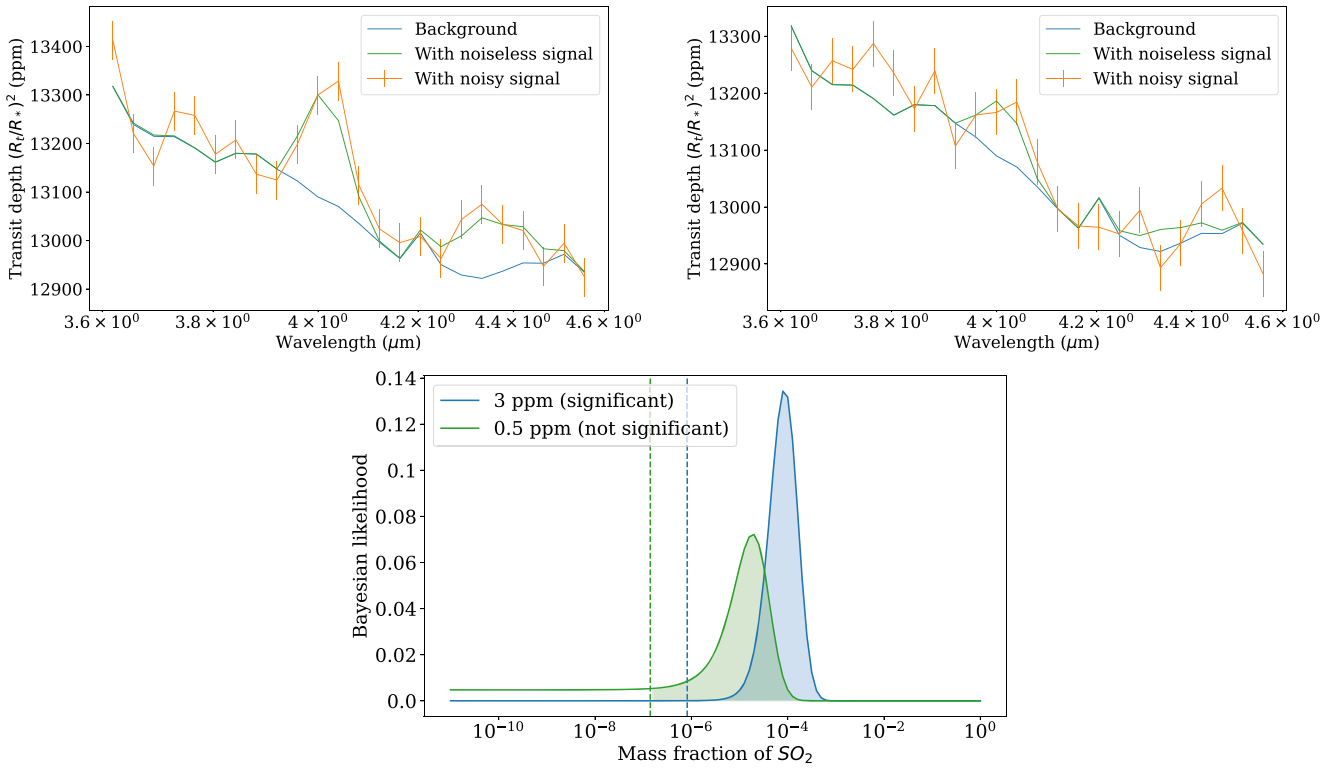

Figure 4. Simulated transmission spectra of a Hycean planet with added abundances of SO_2 above the detection threshold (3 ppm, top left) and below the detection threshold (0.5 ppm, top right), and the SO_2 mass fraction posterior PDF from detection tests (bottom). The spectral feature at 4 μm is targeted by the detection test. The spectra are presented with and without simulated JWST noise, which is used for the detection test. The 1% input, above which the posterior PDF is integrated to calculate the significance of detection, is highlighted with a dotted line in the detection test.

Table 3
Spectral Bands of Prebiosignature Molecules

Wavelength Range (μm)	Prebiosignature Molecules	Other Molecules	Instrument
1.55–1.65	H_2S, NH_3		NIRISS
1.90–2.00	H_2S	H_2O, CO_2	NIRISS
2.10–2.30	NH_3, CH_4		NIRISS
2.65–2.75	NO, H_2S	H_2O, CO_2	NIRISS
2.90–3.10	HCN, C_2H_2, NH_3, HC_3N	CO_2	G395M
3.30–3.50	CH_4, CH_2O		G395M
3.50–3.60	HCN, CH_4		G395M
3.65–3.80	C_2H_2, H_2S		G395M
3.90–4.00	SO_2, HCN		G395M
4.20–4.50	HC_3N, SO_2	CO_2	G395M
4.55–4.65	C_2H_2		G395M
4.70–4.80	HCN, CO		G395M
4.80–5.00	HC_3N, CO		G395M
5.00–6.00	NO	H_2O	MIRI
6.20–6.90	NH_3	H_2O	MIRI
7.10–7.80	HC_3N, SO_2, C_2H_2, HCN, H_2S		MIRI

impact the transmission spectrum and therefore the detection thresholds. The other spectra, which already possess strongly absorbing broadband opacity sources from CH_4, NH_3, H_2O, and HCN, would be less impacted by clouds, but it would still affect detection thresholds.

To quantify the impact of various cloud heights on these detection thresholds, we rerun TriArc with gray cloud decks at various altitudes in various planets. Species with their strongest features in unsaturated regions (like CO in CH_4-dominated atmospheres) are more steeply affected than species in saturated regions (like C_2H_2 in atmospheres containing NH_3). For the hydrogen-rich super-Earth we add a cloud deck at 0.1 bar to represent Earth-like water clouds, and find that detection thresholds increase by a factor of 10–20. For the ultra-reduced volcanic planet, using the same aerosol layer at 10 mbar as Rimmer et al. (2021a) causes a 3–10 times increase in the detection thresholds. To represent a high-altitude organic haze in the 100 kyr post-impact atmosphere we use a 1 mbar cloud deck, greatly flattening the background transmission spectrum and increasing most detection thresholds between 3 and 20 times (3 for C_2H_2, 4 for SO_2, 10 for HCN, 20 for NO), yet 1000 times for CO. For our most extremely cloudy scenario, we use an extremely high-altitude aerosol at 100 μbar cloud deck in the 10 Myr post-impact atmosphere. This creates an effectively flat background transmission spectrum, and the corresponding detection thresholds are purely an expression for the strength of the molecule's strongest feature. Therefore detection thresholds of strong absorbers like HC_3N, C_2H_2, and CH_4 only increase by 100–200 times, while weaker absorbers like SO_2, H_2S, and HCN increase by 2500–6000 times, and both CO and NO become undetectable.

3.3. Retrieval Results

As a consequence of our detection test method, the detection thresholds may not necessarily correspond to the exact minimum abundances that we might obtain from real observations. We may expect our results to be optimistic as we assume perfect knowledge of the exoplanet and the other species in its atmosphere. In a realistic retrieval, any uncertainty in the atmospheric composition or planetary properties will affect the retrieved abundance of trace species.

Table 4
Detection Thresholds of Prebiosignature Molecules in Model Exoplanet Atmospheres, Using Three Transits Per Instrument of GJ 1132b at Spectral Resolution $R = 100$

Molecule	Instrument	Hycean (ppm)	Ultra-reduced Volcanic (ppm)	Super-Earth (ppm)	Post-impact (100 kyr) (ppm)	Post-impact (10 Myr) (ppm)
CH_4	G395M	0.37	0.28	0.46	0.0094	0.0089
HCN	G395M	27	66	1.7	4.4	0.026
C_2H_2	G395M	3.6	55	0.56	1.4	0.0087
NH_3	G395M	5.5	84	2.2	2.8	0.084
	NIRISS	0.55	3.3	0.68	0.88	0.042
	MIRI	69	53	14	8.8	0.084
SO_2	G395M	0.58	14	0.45	3.7	0.028
H_2S	G395M	110	2100	27	280	1.3
	NIRISS	69	130	54	35	4.2
NO	MIRI	360	870	61	40	0.40
CO	G395M	1.3	100	2.1	0.54	0.051
CH_2O	G395M	0.16	9.5	0.024	2.0	0.00075
	MIRI	16	7.5	3.1	1.3	0.012
HC_3N	G395M	0.058	5.6	0.14	0.15	0.0070
	MIRI	87	…	…	150	0.35
NH_3	G395M	35	330	6.8	7.0	0.17

As we are considering detection of trace prebiosignatures, it is reasonable to assume that in practice such observations will be made for planets where the dominant absorbing gases in their atmospheres have already been well constrained.

To verify that prebiosignatures of detection threshold abundances can still be identified in a realistic retrieval, we perform a full retrieval using the retrieval package of `petitRADTRANS` on a simulated NIRSpec G395M observation of a Hycean atmosphere. We use the planetary properties and observational regime described in Section 2, with added abundances of the prebiosignatures HCN, C_2H_2, and SO_2 equal to their detection thresholds (27 ppm, 3.6 ppm, and 0.58 ppm, respectively). The results of the retrieval (see Figure 6 for the best-fit spectrum and Figure 7 for the posterior corner plot) successfully identify all three prebiosignatures at their correct abundances (within 2σ). The retrieval accurately constrains the planetary parameters and background composition (H_2O, CH_4, and NH_3), and places upper limits on the CO and CO_2 abundances, which are not present in the forward model. The retrieval highlights the degeneracy present between C_2H_2 and HCN evident as a weakly correlated tail in the posterior PDF, as the interpretation for the feature at 3 μm is degenerate and can be explained with either molecule. The SO_2 feature is nondegenerate, and its posterior PDF is therefore better constrained.

To demonstrate that the prebiosignatures can be robustly detected and distinguished within an order of magnitude of the TriArc-determined detection threshold, we repeat the retrieval, using 5 times the abundance of the prebiosignatures (HCN, C_2H_2, and SO_2). The posterior corner plot from this retrieval is presented in Figure 8. With the increased prebiosignature abundances, all three prebiosignatures are detected and distinguished with tight abundance constraints. Overlapping bands are therefore demonstrated to be a problem at the detection threshold, but the appearance of nonshared spectral features at slightly higher abundances implies that the disambiguation threshold, even for the highly similar molecules HCN and C_2H_2, is within an order-of-magntitude of the detection threshold.

3.4. Alternative Observational Regimes

We here seek to generalize the analysis of detection thresholds by varying some of the assumed observational parameters. To begin with, we calculate the detection thresholds while varying the number of transits, but otherwise keeping the other observational parameters the same as in the primary regime (GJ 1132 with a three hour baseline). This is done for the Hycean benchmark planet with the detection thresholds of CH_4, NH_3, HCN, HC_3N, C_2H_2, SO_2, and CO, all using the NIRSpec G395M instrument (Figure 9). All of these prebiosignatures are detectable in a single transit. Detection thresholds reduce by a factor of 10–40 by going from 1 to 10 transits.

We also want to explore the impact of observing different stars. As the strength of the signal in transmission spectroscopy is proportional to $\frac{1}{R_*^2}$, only the smallest stars are suitable to atmospheric characterization with JWST. Furthermore, observing brighter stars results in less noise. To quantify these effects, we use noise from a sample of relevant planetary systems: GJ 1132b, TRAPPIST-1e, LTT 1445 Ab, K2-3d, and K2-18b, to calculate the detection threshold of HCN in the model Hycean planet with a variable number of transits (Figure 10). In each case, we use a baseline observing time equal to the duration of three transits for that particular planetary system. As expected, the detection threshold strongly depends on stellar radius, and also depends on the star's magnitude at relevant wavelengths. Regardless of the type of star the detection threshold decreases by approximately the same relative amount with number of transits. HCN is detectable in Hycean LTT 1445 Ab, GJ 1132b, and TRAPPIST-1e with a single transit, two transits are required for K2-18b, and four transits for K2-3d.

We also want to test the efficacy of long duration observing regimes at detecting prebiosignatures in high-mean-molecular-weight atmospheres. The habitable zone planet TRAPPIST-1e is ideally suited to observation and has been observed to lack a cloud-free low-mean-molecular-weight atmosphere (De Wit et al. 2018). In order to explore both the high-mean-molecular-weight atmosphere of early Earth and the TRAPPIST-1 system, we simulate surveys of 5–100 transits around M8V star

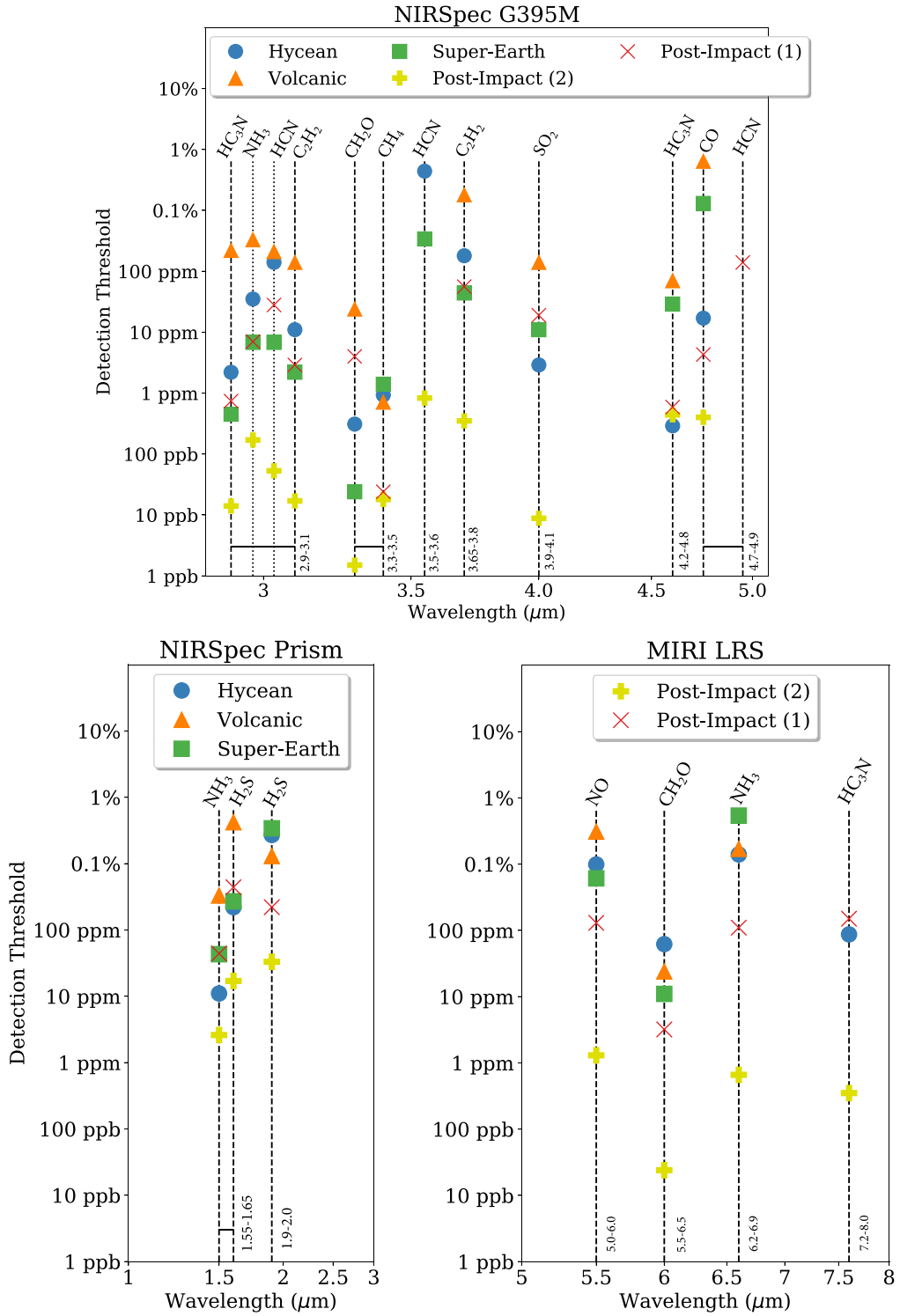

Figure 5. Detection thresholds of prebiosignature molecules at different wavelengths for different model exoplanets. JWST noise is simulated using three transits per instrument of GJ 1132b at spectral resolution $R = 100$. Post-impact (1) refers to the 100 kyr post-impact case and post-impact (2) refers to the 10 Myr post-impact case.

TRAPPIST-1 at spectral resolution $R = 100$ (each with 10 hr of out of transit observation). The noise we obtain from this is used to calculate detection thresholds with a varying number of transits for our model TRAPPIST-1e, with a high-mean-molecular-weight 90% N_2 10% CO_2 atmosphere to simulate the atmosphere of the early Earth (Kaltenegger et al. 2007; Rugheimer et al. 2015). We use a 10 ppm systematic noise floor for our high intensity regimes, which is approached but not reached at any point, even for 100 transits. These results are illustrated in Figure 11.

With five transits, we are able to detect only CH_4 and NH_3 both with the NIRSpec G395M instrument. This concurs with the analysis of Morley et al. (2017), who found the dominant absorbing gas is observable at four transits for TRAPPIST-1e.

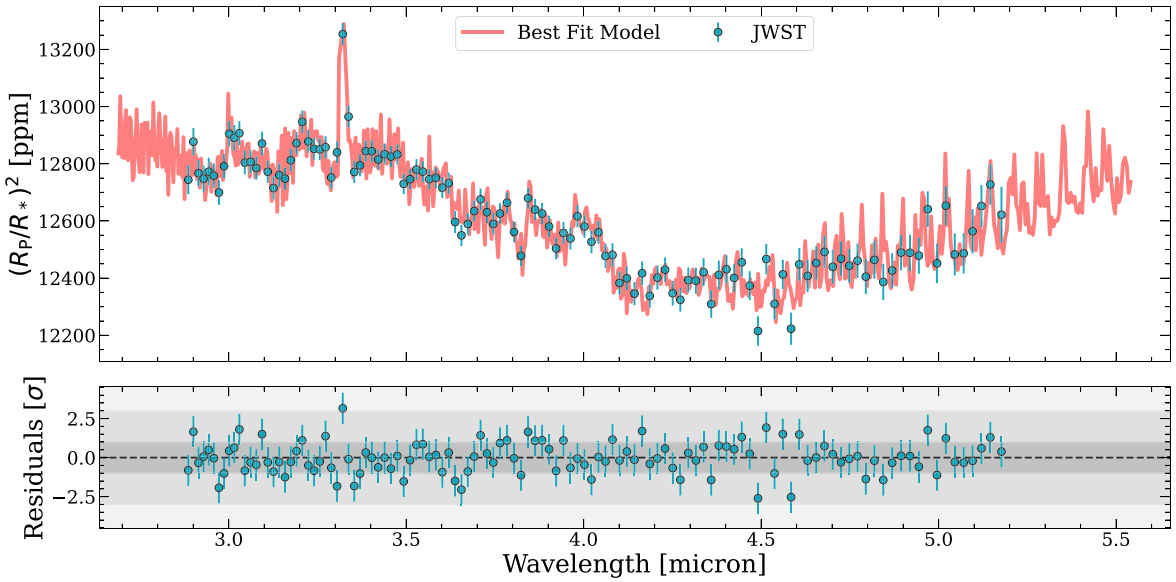

Figure 6. Best-fit transmission spectrum to a simulated NIRSpec G395M observation of a Hycean atmosphere with `TriArc`-calculated detection threshold abundances of three prebiosignatures (HCN, C_2H_2, and SO_2) assuming realistic JWST noise from observing three transits of GJ 1132b, calculated using the retrieval package of `petitRADTRANS`.

At these concentrations, both CH_4 and NH_3 would constitute the dominant absorbing gas. At 7 transits we detect C_2H_2, 9 transits we detect HC_3N, and 10 transits we detect HCN. We detect no more prebiosignatures until SO_2 at 40 transits, NO at 70 transits, and H_2S and CO at 100 transits.

3.5. Degeneracies

HCN and C_2H_2 share the same strongest absorbing spectral feature, from 2.9 to 3.1 μm. This results in a degeneracy, as the presence of HCN would result in the detection of C_2H_2 and vice versa using `TriArc`. These degeneracies can be hard to break and highlight the need to explore other wavelength bands. By retrieving at the next best band (that they do not share) each molecule can be distinguished and further information gathered. We therefore present the detection thresholds at multiple bands in Figure 5, with the non-best-case bands serving as disambiguation thresholds.

In the case of the Hycean planet for example, the C_2H_2 detection threshold is 11 ppm, but the disambiguation threshold is 180 ppm. Therefore, for between 11 and 180 ppm only a detection at 3 μm would be observed (at a 3σ level), so either HCN or C_2H_2 could be responsible for the detection. With $>$180 ppm of C_2H_2, there would also be an observation at 3.7 μm, and the presence of C_2H_2 could be confirmed. The band at 3.5 μm could be explored by integrating the posterior PDF to constrain the maximum abundance of HCN present. The full retrieval, however, finds that while HCN and C_2H_2 are slightly degenerate at their detection thresholds, increasing the abundance by 5$\times$ is sufficient to distinguish between HCN and C_2H_2. Therefore we find that the TriArc method of finding disambiguation thresholds massively overestimates the disambiguation threshold, as it does not use information from multiple spectral features.

This hydrogen cyanide–acetylene degeneracy is the most severe and difficult to break due to the spectroscopic similarity of these molecules, as predicted by Sousa-Silva et al. (2019). There is actually a four-way degeneracy between HCN, C_2H_2 NH_3, and HC_3N at 3 μm, but both NH_3 and HC_3N have other strong spectral features that can be observed, so disambiguation is much easier. The other nontrivial degeneracy is between CH_4 and CH_2O, which possess very similar spectra at NIR wavelengths. These can be distinguished with the detection or nondetection of the feature of CH_2O at 6 μm with MIRI. While the difference between the detection and disambiguation threshold likely varies between pairs of degenerate molecules, no pair that we consider are more degenerate than the highly spectrally similar HCN and C_2H_2.

It is also worth noting that we are also assuming that the abundances of these species are independent, but our background knowledge of the photochemical stability and geophysical plausibility of the molecules could also inform our priors and hence impact our analysis of degeneracies.

The challenge of distinguishing molecular spectral features is a known difficulty in the field of atmospheric characterization, exemplified by the contested detection of phosphine in the atmosphere of Venus (Greaves et al. 2021; Villanueva et al. 2021). Higher spectral resolution can also allow observers to break degeneracies (Tremblay et al. 2020). For all of our calculations we bin to a decreased resolution of $R = 100$, while the G395M instrument is capable of achieving resolutions of $R \approx 1000$. The G395H instrument can achieve an even higher resolution of $R \approx 3400$, at the cost of a gap in the spectrum useful for detecting H_2S and distinguishing C_2H_2 and HCN.

4. Discussion

We have shown that all the prebiosignature molecules we have considered are detectable in hydrogen-rich exoplanets using a modest amount of observation time with JWST. Cyanoacetylene (HC_3N) and formaldehyde (CH_2O) are the most readily detected primary prebiosignatures. Secondary prebiosignatures, CH_4 and C_2H_2, are also particularly well suited to detection, and primary prebiosignatures SO_2, HCN, CO, and NH_3 are detected in trace abundances in most cases. All of these are detected at wavelengths explored with the NIRSpec G395M instrument. Adding in the NIRISS SOSS instrument allows for the detection of H_2S (in moderate to large

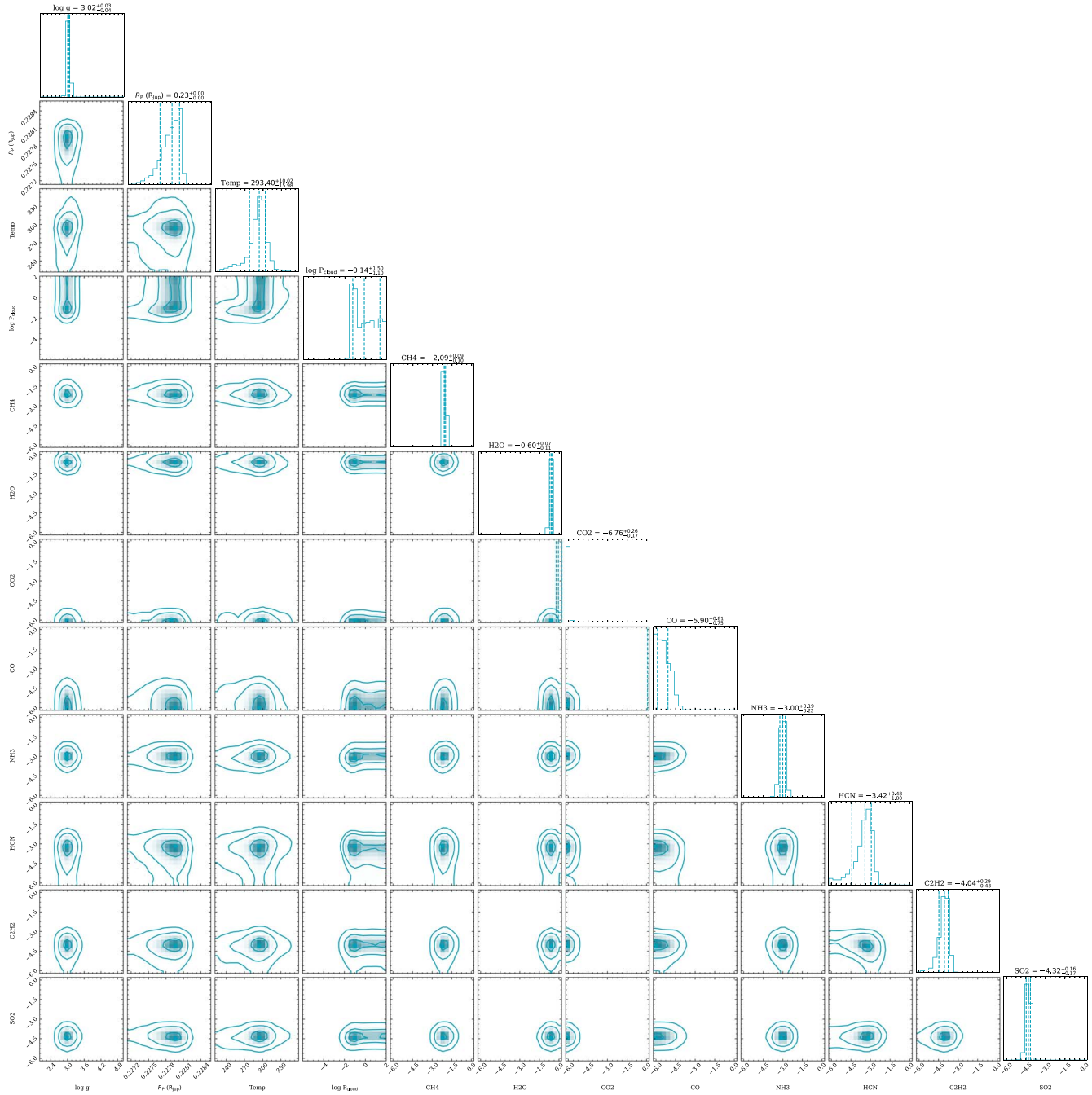

Figure 7. Full posterior distribution from the `petitRADTRANS` retrieval of a simulated NIRSpec G395M observation of a Hycean atmosphere with `TriArc`-calculated detection threshold abundances of three prebiosignatures (HCN, C_2H_2, and SO_2) assuming realistic JWST noise from observing three transits of GJ 1132b. The prebiosignature mass fractions are identified within 2σ of their true values (HCN $= -2.78$, $C_2H_2 = -3.92$, $SO_2 = -4.1$). Due to the overlapping strongest features of HCN, C_2H_2, and NH_3, there is a tail in the posterior PDF of both HCN and C_2H_2 as the interpretation for the shared feature at 3 μm is somewhat degenerate.

abundances) and can aid in the disambiguation of NH_3. Including observation with the MIRI LRS instrument allows the detection of NO (only in large abundances) and is also necessary to distinguish between CH_2O and CH_4.

We present a discussion of the chemical and physical contexts that affect prebiosignatures for each planet in Section 4.1. We discuss the impact of observational parameters and the application to observing strategies in Section 4.2. We also touch on how these can be related to prebiotic chemistry experiments in Section 4.3.

4.1. Impact of Planetary Properties on Detection Thresholds

The primary impact of planetary properties on the detection thresholds is through the scale height. This trend is most readily observed in the detection thresholds for CH_4, as its strong broadband opacity means that it will tend to dominate the transmission spectrum of a planet even in small abundances and avoid being obscured by absorption lines from another molecule. However, for most molecules the detection threshold is significantly lower in more transparent atmospheres with less broadly and strongly absorbing molecules like CO (10 Myr

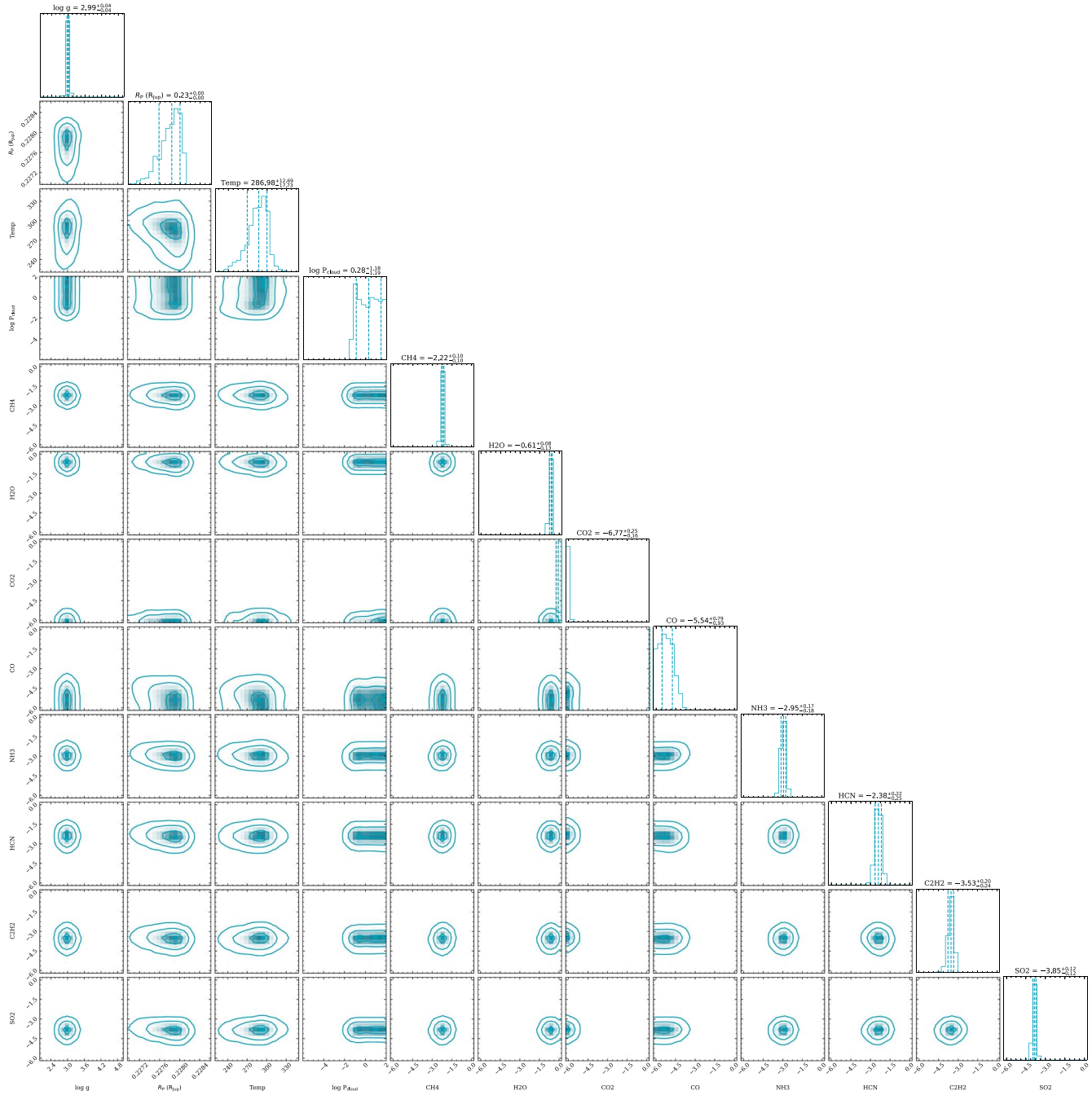

Figure 8. Full posterior distribution from the `petitRADTRANS` retrieval of a simulated NIRSpec G395M observation of a Hycean atmosphere with 5 times the `TriArc`-calculated detection threshold abundances of three prebiosignatures (HCN, C_2H_2, and SO_2) assuming realistic JWST noise from observing three transits of GJ 1132b. The prebiosignature mass fractions are identified within 1–2σ of their true values (HCN $= -2.28$, $C_2H_2 = -3.42$, $SO_2 = -3.6$). With the increased abundances all three prebiosignatures are robustly detected and distinguished, demonstrating the order-of-magnitude accuracy of the detection threshold method.

post-impact planet) and CO_2 (super-Earth) than in the other CH_4-dominated atmospheres. The combination of CH_4 and HCN in particular makes the detection thresholds for the ultrareduced volcanic planet particularly high.

Clouds and hazes can also significantly impact detection thresholds by reducing the strength of absorption features. When decoupled from the assumed planetary radius, a gray cloud deck has an identical impact on detection thresholds as surface pressure. The sensitivity analysis of the impact of the pressure of the cloud deck demonstrates a steep dependence of detection threshold on the cloud-top pressure (or equivalently surface pressure) if they are found above the photosphere at approximately 10 mbar (see the Appendix). In addition to water clouds, prebiosignatures may impact their own observability, through the generation of both photochemical hazes from HCN (such as on Titan, e.g., Lara et al. 1999) and sulfur aerosols (Hu et al. 2013).

4.1.1. Sub-Neptunes and Ocean Planets

As sub-Neptunes are a particularly abundantly discovered type of exoplanet, it would be statistically very advantageous to any prebiosignature (or biosignature) survey if they do constitute a suitable environment for life (Madhusudhan et al.

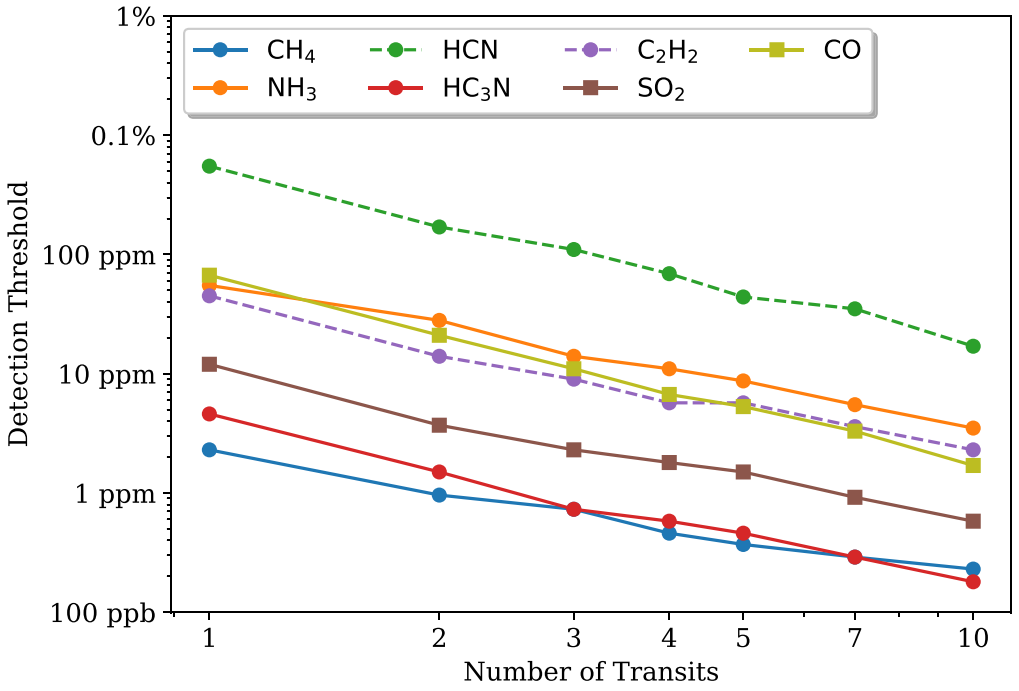

Figure 9. Detection thresholds for prebiosignature molecules with NIRSpec G395M as a function of the number of transits using simulated transmission spectra of a model Hycean exoplanet, with synthetic JWST noise from observing GJ 1132 at spectral resolution $R = 100$.

2021). The detection of water vapor in a low-mean-molecular-weight atmosphere around sub-Neptune K2-18b (Benneke et al. 2019; Tsiaras et al. 2019) is consistent with a range of internal compositions, including a water-rich composition (Madhusudhan et al. 2020). It is unclear whether the planet does indeed have an ocean surface. Scheucher et al. (2020) excluded the existence of an oceanic surface due to the low mean molecular weight of the atmosphere and assumed evaporation from a water surface. For a planet such as K2-18b, it may require a thinner hydrogen envelope, strong cloud cover, or lower instellation to prevent sufficient water evaporation at the surface. JWST-detectable observational discriminants for the existence of a ocean surface beneath a thin envelope for sub-Neptune planets are explored by Tsai et al. (2021). Notably, they find lack of NH_3, detectable with three transits of NIRSpec G395H, would be evidence for lack of an ocean surface. This makes the detection threshold for NH_3 in a Hycean atmosphere that we have found particularly significant in this case, as NH_3 is also both a prebiosignature, and a potential biosignature in hydrogen-dominated atmospheres (Seager et al. 2013b). Interestingly, we find the detection threshold of NH_3 in a Hycean-type atmosphere to be lower at the wavelengths explored by the NIRISS SOSS and G140M instruments, which is helpful to distinguish it from molecules with their dominant feature at 3 μm (like HCN and C_2H_2).

Another consideration for prebiosignature detection on a Hycean planet and other oceanic planets, is the impact of planet-wide oceans on the atmospheric chemistry. Soluble molecules, such as NH_3, CH_2O, and methanol (CH_3OH) would have difficulty accumulating in the atmosphere (e.g., Huang et al. 2022; Zhan et al. 2022). Very large production rates would be required for prebiotically relevant concentrations to develop in the oceans and, depending on the ocean–atmosphere equilibrium, no observable abundance of gas will accumulate in the atmosphere. Pinto et al. (1980) demonstrate how photochemically derived formaldehyde could accumulate in Earth's primitive oceans. The solubility of these species is considered in Section 4.3 to determine what concentrations may build up. Tsai et al. (2021) used CH_3OH as an observational discriminant between a solid and liquid ocean surface in K2-18b, observable with 20 JWST transits using MIRI LRS. Many conventional environments proposed for the origin of life, such as tidal pools (Deamer 1997), impact craters (Chatterjee 2016), carbonate-rich lakes (Toner & Catling 2020), surface hydrothermal vents (Rimmer & Shorttle 2019), and hot springs (Damer & Deamer 2020), could not occur on a planet completely lacking a solid surface.

However, providing sub-Neptunes with liquid water surfaces exist and are not uniformly impacted by high continuous clouds, they greatly add to the sample of planets available to prebiosignature (and biosignature) analysis. They are well suited to detection due to their high scale height, although broad H_2O and CH_4 features do increase the detection thresholds, particularly of HCN and NO. The presence of an ocean surface can be explored simultaneously to prebiosignatures by the detection or nondetection of NH_3.

4.1.2. Super-Earths and Volcanic Planets

Super-Earths are another abundantly detected class of exoplanet. A favored explanation for the bimodal distribution (radius gap) in planetary radii in super-Earth/sub-Neptune mass planets is the presence, or lack of, thick primary envelopes, driven by photoevaporation (e.g., Lammer et al. 2003) or core-powered mass loss (e.g., Ginzburg et al. 2016). Planets that have retained their thick hydrogen envelope are the sub-Neptunes discussed above. Considering planets without a thick hydrogen envelope, we can still expect some super-Earths to possess secondary atmospheres from outgassing during accretion, or later due to tectonic processes (Elkins-Tanton & Seager 2008; Liggins et al. 2020). The higher gravity could

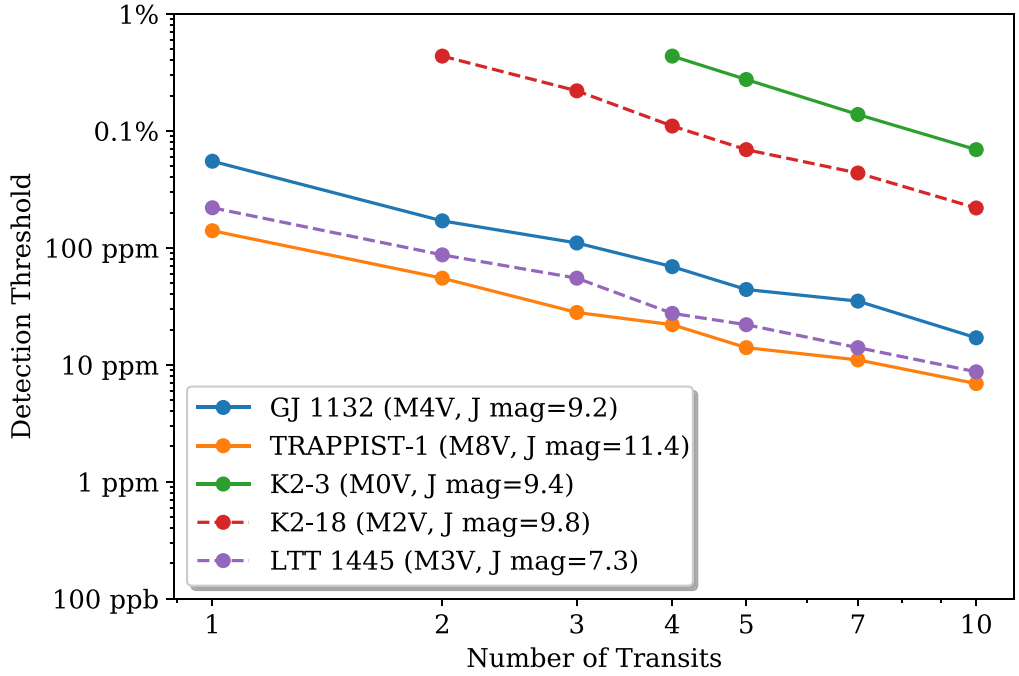

Figure 10. Detection thresholds of HCN as a function of the number of transits for a selection of model stars, using simulated transmission spectra of a model Hycean exoplanet at spectral resolution $R = 100$.

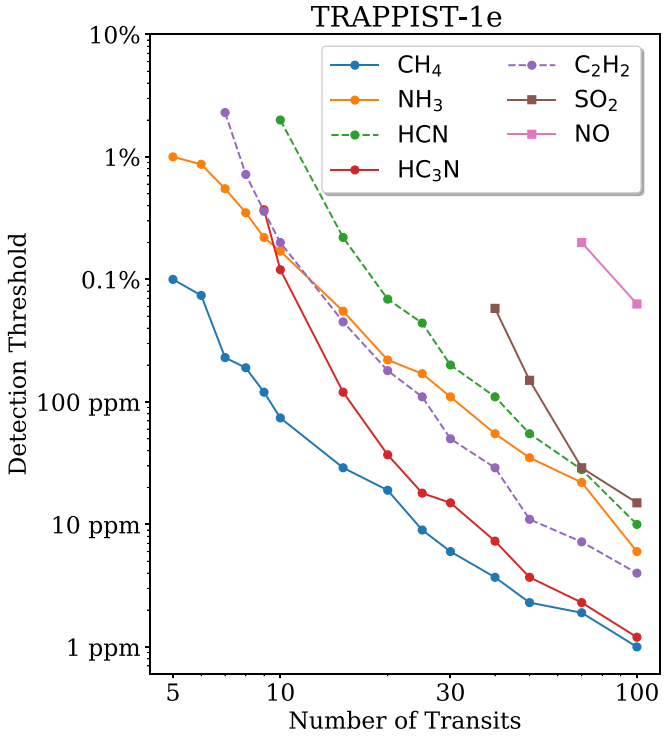

Figure 11. Detection thresholds of prebiosignature molecules as a function of the number of transits using simulated transmission spectra of TRAPPIST-1e with an early-Earth atmosphere at spectral resolution $R = 100$.

allow a planet to retain hydrogen in its atmosphere (Miller-Ricci et al. 2008), and significant hydrogen in-gassing during accretion could buffer mass loss with subsequent outgassing (Chachan & Stevenson 2018). Sulfur species released by volcanism could cause significant aerosol cover that impacts the detectability of other features, but in itself could be an observational discriminant for active volcanism and the presence of prebiosignatures H_2S and SO_2 (Hu et al. 2013; Jordan et al. 2021).

Our modeling of a hydrogen-rich Super-Earth is performed assuming a stable hydrogen- and nitrogen-rich secondary atmosphere. Volcanism can cause carbon species like CO_2 to accumulate to significant quantities, we consider only 100 ppm of CO_2, but both CO and CH_4 could accumulate depending on the nature of the outgassing. If thin hydrogen-rich atmospheres are indeed a common feature of super-Earths, they are ideal candidates for the detection of prebiosignatures, particularly if the primary carbon species is CO_2 or CO, which do not significantly interfere with the detection of most prebiosignature molecules. Even if enriched with higher-mean-molecular-weight components due to hydrogen escape, the sensitivity analysis (Appendix) shows that prebiosignatures remain detectable for hydrogen abundances of around 70%.

The ultrareduced volcanic planet we consider (e.g., Swain et al. 2021), relies on large quantities of hydrogen-rich outgassing to maintain the hydrogen-rich atmosphere, as the hydrogen would otherwise rapidly escape due to the planet's Earth-like gravity. Whether these observations prove to support the presence of a low-mean-molecular-weight atmosphere with HCN is a matter of debate (Mugnai et al. 2021; Libby-Roberts et al. 2022), so the physical relevance of the detection thresholds remains to be seen. However, if confirmed with JWST observations, it highlights volcanism on some planets as a potential rich source of prebiotically relevant chemicals, detectable on a planetary scale. Both the observations of Swain et al. (2021) and modeling of Rimmer et al. (2021a) suggest the presence of aerosols or hazes composed of carbon–nitrogen species like on Titan (Clarke & Ferris 1997), which would further raise the already high detection thresholds. The surface temperature on GJ 1132b is also likely to be above that suitable for prebiotic chemistry. It is therefore highly uncertain how

significant this hypothetical class of planet is to an overall study of the origin of life on exoplanets.

4.1.3. Post-impact Planets

The inherent transience of an impact-derived atmosphere makes it unclear how frequently we could expect to detect post-impact planets. The exact nature of the post-impact atmosphere is also sensitive to both the initial size and composition of the impacted planet, and the size and composition of the impactor, as well as the time since the impact (Zahnle et al. 2020), but can be generalized as either recent (CH_4-dominated) or late (CO-dominated). Subsequent atmospheric evolution also depends on interactions of the impact-generated atmosphere with the now molten surface, which can lead to less reducing atmospheres than the ones we used in our prebiosignature analysis (Itcovitz et al. 2022).

The recent post-impact condition (represented in our models by the 100 kyr post-impact planet, but the exact length of the time the condition persists is sensitive to many parameters, in particular stratospheric H_2O abundance) is extremely well suited to prebiotic chemistry, with prebiotic chemicals like HCN and CH_4 present in the atmosphere. However, it suffers from the issue that the surface temperature will likely exceed those allowed for most prebiotic syntheses. Furthermore detectability thresholds are likely to be reduced by photochemical hazes and aerosols, and this post-impact state does not last long so may not be well-represented in the exoplanet population.

The later post-impact state (represented in our models by the 10 Myr post-impact planet), where the atmosphere is predominantly H_2 and CO, is exceptionally good for the detection of trace species. With a carbon to oxygen ratio (C:O) of approximately unity, prebiotic species like HCN can be formed from lightning, impacts, and stellar activity (Rimmer & Rugheimer 2019). This state also persists for a considerable length of time, with steadily decreasing abundances of hydrogen due to escape processes, favoring the discovery of an exoplanet in such a state. The surface temperature is likely to be more temperate than in the earlier atmospheric evolution, but may still be hostile to prebiotic chemistry due to the greenhouse effect of H_2 (Pierrehumbert & Gaidos 2011). Overall, if we discount their possible rarity, post-impact planets are ideal targets for detecting prebiosignatures.

4.1.4. Early Earth

High-mean-molecular-weight atmospheres on exoplanets around red dwarfs are not beyond the realm of study of JWST, but require significant observation time. There are also very few known planetary systems amenable to such a study (Morley et al. 2017). The most promising candidate planet, TRAPPIST-1e, has accessible detection thresholds for CH_4, NH_3, HCN, HC_3N, and C_2H_2 with 5–10 transits, but other prebiosignatures require a perhaps prohibitively long observation program (40–100 transits). Should initial observations of TRAPPIST-1e or another TRAPPIST-1 planet prove fruitful, we may find ourselves devoting significant observation time to the TRAPPIST-1 system. Beyond this system we will need to focus on finding prebiosignatures in hydrogen-rich atmospheres (with JWST at least), rather than early-Earth or other solar system atmosphere analogs. The study of early-Earth atmospheres in exoplanets is a task better suited to future observatories.

4.2. Impact of Observing Strategy on Prebiosignature Detection

The detection thresholds we have calculated are sensitive to the duration of observing time, as well as the radius and magnitude of the observed star. The detection threshold decreases with the number of transits at a roughly constant rate in log–log space. The slope of the dependence on detection threshold on the number of transits depends on the species in question (Figure 9), but largely does not depend on the star when considering M dwarfs (Figure 10). A systematic noise floor, such as that found by Rustamkulov et al. (2022), will cause the detection threshold to eventually level off, which will happen with fewer transits for brighter stars. Prebiosignatures in hydrogen-rich atmospheres are feasibly detected in five transits in M dwarfs of 10th *J* magnitude or less. Brighter late K dwarfs are feasible targets, as are smaller and dimmer M dwarfs, notably including TRAPPIST-1 and Kepler-1649 (Vanderburg et al. 2020). The precise number of transits that is ideal for any particular planetary system will depend on the star, the planetary properties, and the desired detection threshold. For example, high-mean-molecular-weight atmospheres are moderately well characterized in the case of very small stars (e.g., TRAPPIST-1) after 10 transits, but detection of all prebiosignatures in these atmospheres requires 100 transits (Figure 11).

By far the most important JWST instrument for prebiosignature detection is NIRSpec G395M (or G395H), as the most important spectral features for CH_4, C_2H_2, HC_3N, HCN, CO, SO_2, and NH_3 all exist in the 2.9–5 μm range. A more conservative observational regime could use NIRSpec G395M exclusively (potentially combined with a single transit of NIRISS SOSS to enhance atmospheric retrievals). This would sacrifice the ability to detect NO (which requires MIRI LRS) and H_2S (which requires NIRSpec Prism, NIRISS SOSS, or NIRSpec G140M), and to disambiguate molecules like CH_4 from CH_2O, and potentially HCN from NH_3. For the 1–2.9 μm range, NIRISS SOSS, or NIRSpec Prism should be used depending on the brightness of the target. The wider spectral baseline of these instruments makes them more attractive than using the NIRSpec G140M instrument when performing retrievals, even though we do not find any detection or disambiguation thresholds in the 2–2.9 μm range.

4.3. Prebiotic Consequences of the Detection Thresholds

The prebiosignatures that we focus on here are relevant for prebiotic chemistry that takes place in water. The "success" of the prebiotic chemistry depends critically on the concentration of these species in liquid water, and there is a close but complex relationship between atmospheric and surface water concentrations. This relationship depends on the local geochemistry of these waters. Drawing the connection between global atmospheric partial pressures of a molecule and expected global and local concentrations of that same molecule is outside the scope of this paper.

Aqueous concentrations are most relevant for primary prebiosignatures: species that participate directly in the chemical synthesis of prebiotically relevant compounds. The atmospheric partial pressures of secondary biosignatures:

species that indicate events and/or environmental factors that may be conducive for certain prebiotic chemical scenarios (e.g., lightning, giant impacts, volcanism), are related to the ubiquity and intensity of these processes, and these relations have been worked out for several secondary prebiosignatures (e.g., Kaltenegger & Sasselov 2009; Rimmer & Rugheimer 2019; Rimmer et al. 2019, 2021a, 2021b).

5. Conclusion

We have described the creation of a pipeline to compute the minimum abundance of a molecule required in an exoplanet atmosphere to be detected by JWST. Using this pipeline we have have computed the JWST detection thresholds for ten prebiosignature molecules in a selection of model exoplanets. We have varied the observational regime by choosing different stars and number of transits to quantify the effect this has on the detection thresholds. We discussed how these results relate to the relevance of prebiosignature detection with each model exoplanet we used and how they could inform observing strategies when attempting to detection prebiosignatures.

Our key finding is that the study of prebiosignatures and the origin of life in an exoplanetary context is well within the capabilities of JWST, in the case of a low-mean-molecular-weight atmosphere or an optimal target system (like TRAPPIST-1). All 10 of our prebiosignatures are detectable in all the hydrogen-rich atmospheres we consider, using a modest number of transits (<5) and applicable to a reasonable number of target stars. Notably, quantities of HCN, H_2S, or HC_3N, species at the heart of the cyanosulfidic and other prebiotic scenarios, are well detected as atmospheric species. We can therefore directly constrain these scenarios with observations. Secondary prebiosignatures C_2H_2, CH_4, and CO are frequently detectable in very low abundances on the order of a few ppm, which may help constrain both prebiotic chemistry, atmospheric redox, and other relevant processes including impacts and volcanism. We also have well-constrained detection thresholds for gaseous SO_2, NO, and NH_3, which will be strongly related to the aqueous chemistry of surface waters. For the most part, we find that high-mean-molecular-weight atmospheres (such as that of early Earth) are not suitable to the detection of prebiosignatures, but we do find that in the case of TRAPPIST-1e, many prebiosignatures are detectable with 10 transits. TRAPPIST-1, and similar ultracool stars like SPECULOOS-2 (Delrez et al. 2022), are therefore our most immediate avenue with which we might explore Earth-like atmospheres. The tools we have developed in this paper give the opportunity to repeat this kind of detection threshold analysis for any situation where detection of a trace amount of an atmospheric species would be interesting. Beyond prebiosignatures, this has obvious applications to biosignatures and other atmospheric processes.

JWST has proven a powerful tool in the remote sensing of exoplanet atmospheres, having already made novel discoveries of CO_2 and SO_2 in the atmosphere of WASP-39b (The JWST Transiting Exoplanet Community Early Release Science Team et al. 2023; Ahrer et al. 2023; Alderson et al. 2023; Feinstein et al. 2023; Rustamkulov et al. 2023). Notably the detection of SO_2 is evidence for photochemistry (Tsai et al. 2023), and is a prebiosignature in appropriate planetary contexts.

Furthermore, many of the planets we have discussed as suitable for prebiosignature analysis, including the TRAPPIST-1 planets, GJ 1132b, LTT 1445 Ab, and K2-18b are all targets of the JWST GO Cycle 1 or GTO programs. We therefore expect a wealth of data about the atmospheres of these planets, which may even include the detection of prebiosignature molecules, and should certainly help understand the atmospheric contexts present in terrestrial planets. Follow-up observations to further characterize the atmosphere may yield highly useful data of great prebiotic relevance, able to confirm or rule out the presence of prebiosignatures. Even if JWST observations of terrestrial planets yield flat spectra, as seen in recent shorter-wavelength observations of GJ 1132b (Libby-Roberts et al. 2022), LTT 1445 Ab (Diamond-Lowe et al. 2023), and L98-59b (Damiano et al. 2023), we can still expect to study relevant atmospheric processes to the origin of life with JWST by observating temperate and warm planets with significant hydrogen envelopes. Looking beyond JWST, the wavelength range that we consider also overlaps with the wavelengths considered by LIFE (4–18 μm), so detection of prebiosignatures in directly imaged Earth-like planets may be possible in the future.

The authors would like to thank J. Itcovitz for his feedback and data regarding post-impact atmospheres, and P. Wheatley for his comments and advice. A.B.C. acknowledges support from the Institute of Astronomy and the UK Science and Technology Facilities Council (STFC). P.B.R. thanks the Simons Foundation for support under SCOL award 59963. S.R. acknowledges support from the Glasstone Foundation and of the Natural Sciences and Engineering Research Council of Canada (NSERC) Discovery Grant [2022-04588].

Software: `petitRADTRANS` (Mollière et al. 2019), `PandExo` (Batalha et al. 2017), `TriArc`,[10] `exo-k` (Leconte 2021).

Appendix
Sensitivity Analysis

In order to explore the sensitivity of the detection thresholds to single key parameters, we use the detection of C_2H_2 at 3 μm as a benchmark. In each case we vary a single parameter, holding all others as the constant values described for the model Hycean planet with three transits around GJ 1132b. The parameters that varied are mean the molecular weight (by changing the fraction of nonabsorbing species H_2, He, N_2), isothermal atmosphere temperature, instrument spectral precision, surface pressure, and planet radius. The mean molecular weight and temperature (along with the surface gravity) determine the scale height, which along with the planet radius determines the signal strength of spectral features. The high sensitivity of the detection thresholds to these parameters can be seen in Figure A1, varying by a factor of 10 over the range of reasonable temperatures, and a factor of 5 over the range of reasonable planetary radii. The importance of the mean molecular weight (and hence the hydrogen abundance), which can reasonably range from 2 to 24, is highlighted.

The sensitivity analysis also demonstrates the importance of the surface pressure, or cloud-top pressure in the case of a gray opaque cloud deck. Above the photosphere, found in this case at about 10 mbar, the detection threshold is constant and does not depend on the surface/cloud-top pressure. In the case of a thin atmosphere, with a surface/cloud-top pressure of less than 10 mbar, the detection threshold decreases steeply with

[10] https://github.com/ExoArcturus/TriArc

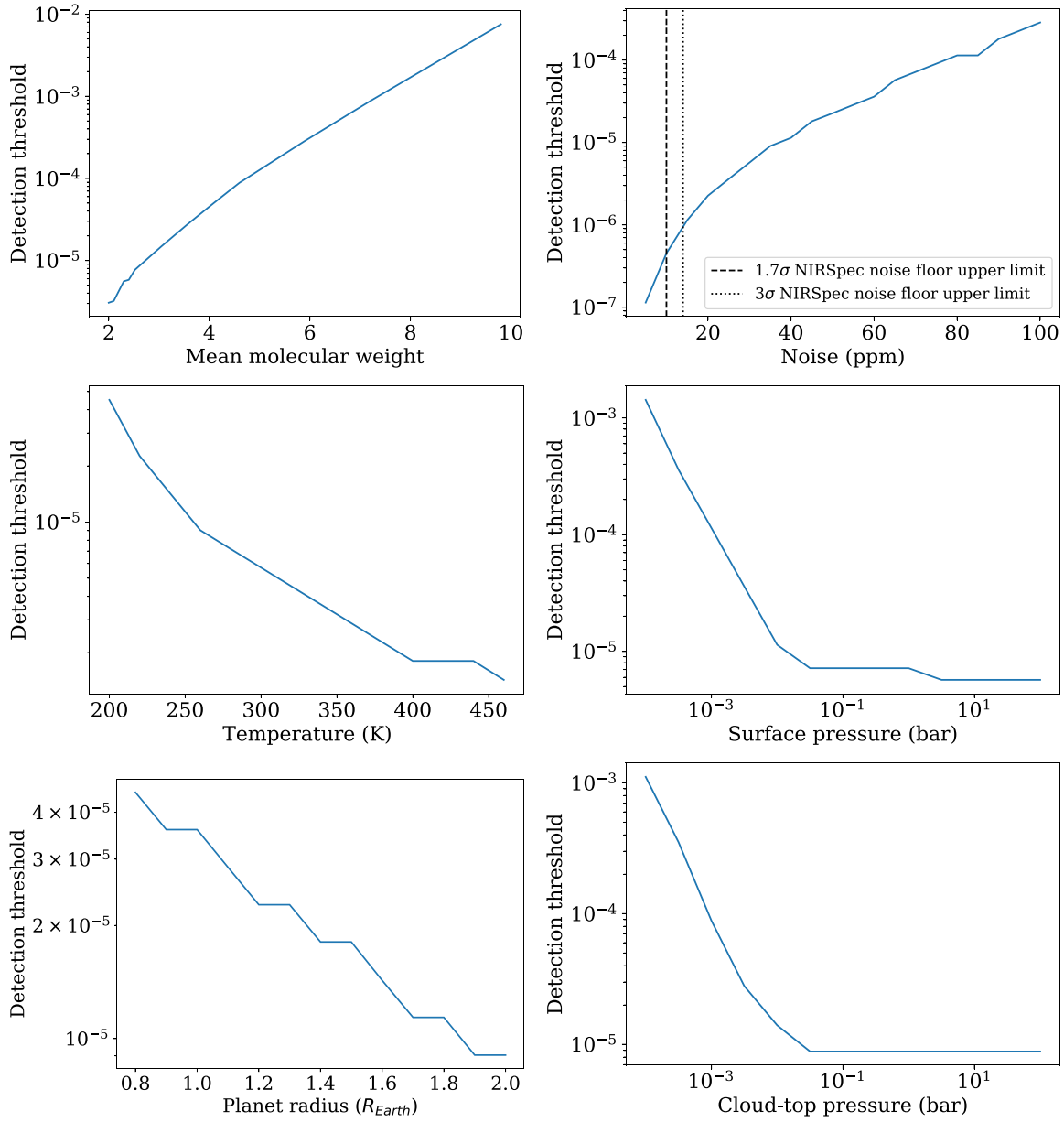

Figure A1. Detection threshold of C_2H_2 as a function of the atmosphere's mean molecular weight (top left), transmission spectrum noise (top right), temperature of the isothermal atmosphere (middle left), surface atmospheric pressure (middle right), planet radius (bottom left), and cloud-top pressure (bottom right). In each case only a single parameter is varied, with other parameters given by a model Hycean planet with noise from observing GJ 1132b for three transits. The noise floors for NIRSpec is given by Rustamkulov et al. (2022).

decreasing surface pressure. Therefore both high cloud and thin atmospheres can both significantly impact detection thresholds by suppressing spectral features (e.g., Kreidberg et al. 2014). The strong dependence of the detection threshold on instrument noise is responsible for the improvements that come from observing increasing numbers of transits, with the JWST noise floor upper limits found by Rustamkulov et al. (2022).

ORCID iDs

A. B. Claringbold https://orcid.org/0000-0003-1309-5558
P. B. Rimmer https://orcid.org/0000-0002-7180-081X
S. Rugheimer https://orcid.org/0000-0003-1620-7658

References

Ahrer, E.-M., Stevenson, K. B., Mansfield, M., et al. 2023, Natur, 614, 653
Airapetian, V., Glocer, A., Gronoff, G., Hebrard, E., & Danchi, W. 2016, NatGe, 9, 452
Alderson, L., Wakeford, H. R., Alam, M. K., et al. 2023, Natur, 614, 664
Alei, E., Konrad, B. S., Angerhausen, D., et al. 2022, A&A, 665, A106
Al-Refaie, A. F., Yachmenev, A., Tennyson, J., & Yurchenko, S. N. 2015, MNRAS, 448, 1704
Angerhausen, D., Ottiger, M., Dannert, F., et al. 2023, AsBio, 23, 183
Azzam, A. A., Tennyson, J., Yurchenko, S. N., & Naumenko, O. V. 2016, MNRAS, 460, 4063
Barber, R., Strange, J., Hill, C., et al. 2014, MNRAS, 437, 1828
Barstow, J. K., & Irwin, P. G. 2016, MNRAS: Letters, 461, L92
Batalha, N. E., Lewis, N. K., Line, M. R., Valenti, J., & Stevenson, K. 2018, ApJL, 856, L34
Batalha, N. E., & Line, M. R. 2017, AJ, 153, 151
Batalha, N. E., Mandell, A., Pontoppidan, K., et al. 2017, PASP, 129, 064501

Benneke, B., Wong, I., Piaulet, C., et al. 2019, ApJL, 887, L14
Benner, S. A., Bell, E. A., Biondi, E., et al. 2020, ChemSystemsChem, 2, e1900035
Berta, Z. K., Charbonneau, D., Désert, J.-M., et al. 2012, ApJ, 747, 35
Butlerow, A. M. 1861, CR, 53, 145
Chachan, Y., & Stevenson, D. J. 2018, ApJ, 854, 21
Charbonneau, D., Brown, T. M., Noyes, R. W., & Gilliland, R. L. 2002, ApJ, 568, 377
Chatterjee, S. 2016, PCCP, 18, 20033
Chubb, K. L., Tennyson, J., & Yurchenko, S. N. 2020, MNRAS, 493, 1531
Clarke, D. W., & Ferris, J. P. 1997, Icar, 127, 158
Cleaves, H. J., II 2008, PreR, 164, 111
Coles, P. A., Yurchenko, S. N., & Tennyson, J. 2019, MNRAS, 490, 4638
Damer, B., & Deamer, D. 2020, AsBio, 20, 429
Damiano, M., Hu, R., Barclay, T., et al. 2023, AsBio, 23, 183
De Wit, J., Wakeford, H. R., Lewis, N. K., et al. 2018, NatAs, 2, 214
Deamer, D. W. 1997, MMBR, 61, 239
Delrez, L., Murray, C., Pozuelos, F., et al. 2022, A&A, 667, A59
Des Marais, D. J., Harwit, M. O., Jucks, K. W., et al. 2002, AsBio, 2, 153
Diamond-Lowe, H., Mendonca, J. M., Charbonneau, D., & Buchhave, L. A. 2023, AJ, 165, 169
Dressing, C. D., & Charbonneau, D. 2015, ApJ, 807, 45
Elkins-Tanton, L. T., & Seager, S. 2008, ApJ, 685, 1237
Feinstein, A. D., Radica, M., Welbanks, L., et al. 2023, Natur, 614, 670
Ferris, J. P., Sanchez, R. A., & Orgel, L. E. 1968, JMB, 33, 693
Ferus, M., Pietrucci, F., Saitta, A., et al. 2019, A&A, 626, A52
Ferus, M., Rimmer, P., Cassone, G., et al. 2020, AsBio, 20, 1476
Fortney, J. J., Marley, M. S., & Barnes, J. W. 2007, ApJ, 659, 1661
Gardner, J. P., Mather, J. C., Clampin, M., et al. 2006, SSRv, 123, 485
Gillon, M., Jehin, E., Lederer, S. M., et al. 2016, Natur, 533, 221
Ginzburg, S., Schlichting, H. E., & Sari, R. 2016, ApJ, 825, 29
Greaves, J. S., Richards, A. M., Bains, W., et al. 2021, NatAs, 5, 655
Green, N. J., Xu, J., & Sutherland, J. D. 2021, JAChS, 143, 7219
Hardegree-Ullman, K. K., Zink, J. K., Christiansen, J. L., et al. 2020, ApJS, 247, 28
Heays, A. N., Kaiserová, T., Rimmer, P. B., et al. 2022, JGRE, 127, e2021JE006842
Hu, R., Seager, S., & Bains, W. 2012, ApJ, 761, 166
Hu, R., Seager, S., & Bains, W. 2013, ApJ, 769, 6
Huang, J., Seager, S., Petkowski, J. J., Ranjan, S., & Zhan, Z. 2022, AsBio, 22, 171
Huang, J., Seager, S., Petkowski, J. J., Zhan, Z., & Ranjan, S. 2022, ApJ, 933, 6
Husser, T.-O., Wende-von Berg, S., Dreizler, S., et al. 2013, A&A, 553, A6
Itcovitz, J. P., Rae, A. S., Citron, R. I., et al. 2022, PSJ, 3, 115
Jakobsen, P., Ferruit, P., de Oliveira, C. A., et al. 2022, A&A, 661, A80
Jordan, S., Rimmer, P. B., Shorttle, O., & Constantinou, T. 2021, ApJ, 922, 44
Kaltenegger, L., & Sasselov, D. 2009, ApJ, 708, 1162
Kaltenegger, L., Selsis, F., Fridlund, M., et al. 2010, AsBio, 10, 89
Kaltenegger, L., Traub, W. A., & Jucks, K. W. 2007, ApJ, 658, 598
Kasting, J. F., & Pollack, J. B. 1983, Icar, 53, 479
Khanna, R. 2005, Icar, 178, 165
Konopacky, Q. M., Barman, T. S., Macintosh, B. A., & Marois, C. 2013, Sci, 339, 1398
Konrad, B., Alei, E., Quanz, S., et al. 2022, A&A, 664, A23
Kreidberg, L., Bean, J. L., Désert, J.-M., et al. 2014, Natur, 505, 69
Krissansen-Totton, J., Bergsman, D. S., & Catling, D. C. 2016, AsBio, 16, 39
Krissansen-Totton, J., Garland, R., Irwin, P., & Catling, D. C. 2018, AJ, 156, 114
Lammer, H., Kasting, J. F., Chassefière, E., et al. 2008, SSRv, 139, 399
Lammer, H., Selsis, F., Ribas, I., et al. 2003, ApJL, 598, L121
Lara, L.-M., Lellouch, E., & Shematovich, V. 1999, A&A, 341, 312
Leconte, J. 2021, A&A, 645, A20
Libby-Roberts, J. E., Berta-Thompson, Z. K., Diamond-Lowe, H., et al. 2022, AJ, 164, 59
Lienhard, F., Queloz, D., Gillon, M., et al. 2020, MNRAS, 497, 3790
Liggins, P., Jordan, S., Rimmer, P. B., & Shorttle, O. 2022, JGRE, 127, e07123
Liggins, P., Shorttle, O., & Rimmer, P. B. 2020, E&PSL, 550, 116546
Liu, Z., Wu, L.-F., Kufner, C. L., et al. 2021, NatCh, 13, 1126
Lustig-Yaeger, J., Meadows, V. S., & Lincowski, A. P. 2019, AJ, 158, 27
Madhusudhan, N., Nixon, M. C., Welbanks, L., Piette, A. A., & Booth, R. A. 2020, ApJL, 891, L7
Madhusudhan, N., Piette, A. A., & Constantinou, S. 2021, ApJ, 918, 1
Miller, S. L. 1953, Sci, 117, 528
Miller, S. L., & Bada, J. L. 1988, Natur, 334, 609
Miller-Ricci, E., Seager, S., & Sasselov, D. 2008, ApJ, 690, 1056
Miyakawa, S., Yamanashi, H., Kobayashi, K., Cleaves, H. J., & Miller, S. L. 2002, PNAS, 99, 14628
Mollière, P., Wardenier, J., van Boekel, R., et al. 2019, A&A, 627, A67
Morley, C. V., Kreidberg, L., Rustamkulov, Z., Robinson, T., & Fortney, J. J. 2017, ApJ, 850, 121
Mugnai, L. V., Modirrousta-Galian, D., Edwards, B., et al. 2021, AJ, 161, 284
Mvondo, D. N., Navarro-González, R., McKay, C. P., Coll, P., & Raulin, F. 2001, AdSpR, 27, 217
Okamura, H., Becker, S., Tiede, N., et al. 2019, ChCom, 55, 1939
Oró, J., & Kimball, A. 1961, Arch. Biochem., 94, 217
Patel, B. H., Percivalle, C., Ritson, D. J., Duffy, C. D., & Sutherland, J. D. 2015, NatCh, 7, 301
Pierrehumbert, R., & Gaidos, E. 2011, ApJL, 734, L13
Pierrehumbert, R. T. 2010, Principles of Planetary Climate (Cambridge: Cambridge Univ. Press)
Pinto, J. P., Gladstone, G. R., & Yung, Y. L. 1980, Sci, 210, 183
Quanz, S. P., Ottiger, M., Fontanet, E., et al. 2022, A&A, 664, A21
Quanz, S. P., Ottiger, M., Fontanet, E., et al. 2022, A&A, 664, A21
Ramirez, R. M., & Kaltenegger, L. 2017, ApJL, 837, L4
Ranjan, S., Wordsworth, R., & Sasselov, D. D. 2017, ApJ, 843, 110
Rauer, H., Gebauer, S. v., Paris, P. v., et al. 2011, A&A, 529, A8
Rigby, J. R., Perrin, M., McElwain, M. W., et al. 2023, PASP, 135, 048001
Rimmer, P., Ferus, M., Waldmann, I., et al. 2019, ApJ, 888, 21
Rimmer, P. B., Majumdar, L., Priyadarshi, A., Wright, S., & Yurchenko, S. 2021a, ApJL, 921, L28
Rimmer, P. B., Ranjan, S., & Rugheimer, S. 2021b, Elements: An International Magazine of Mineralogy, Geochemistry, and Petrology, 17, 265
Rimmer, P. B., & Rugheimer, S. 2019, Icar, 329, 124
Rimmer, P. B., & Shorttle, O. 2019, Life, 9, 12
Rimmer, P. B., Xu, J., Thompson, S. J., et al. 2018, SciA, 4, eaar3302
Rocchetto, M., Waldmann, I., Venot, O., Lagage, P.-O., & Tinetti, G. 2016, ApJ, 833, 120
Rothman, L. S., Gordon, I., Barber, R., et al. 2010, JQSRT, 111, 2139
Rugheimer, S., & Kaltenegger, L. 2018, ApJ, 854, 19
Rugheimer, S., Kaltenegger, L., Zsom, A., Segura, A., & Sasselov, D. 2013, AsBio, 13, 251
Rugheimer, S., Segura, A., Kaltenegger, L., & Sasselov, D. 2015, ApJ, 806, 137
Rustamkulov, Z., Sing, D., Mukherjee, S., et al. 2023, Natur, 614, 659
Rustamkulov, Z., Sing, D. K., Liu, R., & Wang, A. 2022, ApJL, 928, L7
Sagan, C., Thompson, W. R., & Khare, B. N. 1992, Acc. Chem. Res., 25, 286
Scalo, J., Kaltenegger, L., Segura, A., et al. 2007, AsBio, 7, 85
Scheucher, M., Wunderlich, F., Grenfell, J. L., et al. 2020, ApJ, 898, 44
Schlesinger, G., & Miller, S. L. 1983, JMolE, 19, 383
Schwartz, A. W., & De Graaf, R. 1993, JMolE, 36, 101
Schwieterman, E. W., Kiang, N. Y., Parenteau, M. N., et al. 2018, AsBio, 18, 663
Seager, S., Bains, W., & Hu, R. 2013a, ApJ, 775, 104
Seager, S., Bains, W., & Hu, R. 2013b, ApJ, 777, 95
Seager, S., Bains, W., & Petkowski, J. 2016, AsBio, 16, 465
Segura, A., Kasting, J. F., Meadows, V., et al. 2005, AsBio, 5, 706
Shields, A. L., Ballard, S., & Johnson, J. A. 2016, PhR, 663, 1
Sousa-Silva, C., Petkowski, J. J., & Seager, S. 2019, PCCP, 21, 18970
Southworth, J., Mancini, L., Madhusudhan, N., et al. 2017, AJ, 153, 191
Stevenson, K. B., Harrington, J., Nymeyer, S., et al. 2010, Natur, 464, 1161
Sutherland, J. D. 2016, Angew. Chem. Int. Ed., 55, 104
Swain, M. R., Estrela, R., Roudier, G. M., et al. 2021, AJ, 161, 213
Tennyson, J., Yurchenko, S. N., Al-Refaie, A. F., et al. 2016, JMoSp, 327, 73
The JWST Transiting Exoplanet Community Early Release Science Team, Ahrer, E., Alderson, L., et al. 2023, Natur, 614, 649
Tian, F., Toon, O. B., Pavlov, A. A., & De Sterck, H. 2005, Sci, 308, 1014
Toner, J. D., & Catling, D. C. 2020, PNAS, 117, 883
Tremblay, L., Line, M. R., Stevenson, K., et al. 2020, AJ, 159, 117
Tsai, S.-M., Innes, H., Lichtenberg, T., et al. 2021, ApJL, 922, L27
Tsai, S.-M., Lee, E. K., Powell, D., et al. 2023, Natur, 617, 483
Tsiaras, A., Rocchetto, M., Waldmann, I., et al. 2016, ApJ, 820, 99
Tsiaras, A., Waldmann, I. P., Tinetti, G., Tennyson, J., & Yurchenko, S. N. 2019, NatAs, 3, 1086
Underwood, D. S., Tennyson, J., Yurchenko, S. N., et al. 2016, MNRAS, 459, 3890
Vanderburg, A., Rowden, P., Bryson, S., et al. 2020, ApJL, 893, L27
Villanueva, G., Cordiner, M., Irwin, P., et al. 2021, NatAs, 5, 631
Winters, J. G., Medina, A. A., Irwin, J. M., et al. 2019, AJ, 158, 152
Wong, A., Yurchenko, S. N., Bernath, P., et al. 2017, MNRAS, 470, 882
Wunderlich, F., Godolt, M., Grenfell, J. L., et al. 2019, A&A, 624, A49
Wunderlich, F., Scheucher, M., Grenfell, J. L., et al. 2021, A&A, 647, A48

Xu, J., Ritson, D. J., Ranjan, S., et al. 2018, ChCom, 54, 5566
Yurchenko, S., Mellor, T. M., Freedman, R. S., & Tennyson, J. 2020, MNRAS, 496, 5282
Yurchenko, S. N., Amundsen, D. S., Tennyson, J., & Waldmann, I. P. 2017, A&A, 605, A95
Zahnle, K. J., & Catling, D. C. 2017, ApJ, 843, 122
Zahnle, K. J., Lupu, R., Catling, D. C., & Wogan, N. 2020, PSJ, 1, 11
Zhan, Z., Huang, J., Seager, S., Petkowski, J. J., & Ranjan, S. 2022, ApJ, 930, 133